Thermal conductivity of glasses

A structural point of view

Sørensen, Søren Strandskov

DOI (link to publication from Publisher):
10.54337/aau504485511

Publication date:
2022

Document Version
Publisher's PDF, also known as Version of record

THERMAL CONDUCTIVITY OF GLASSES: A STRUCTURAL POINT OF VIEW

BY
SØREN STRANDSKOV SØRENSEN

DISSERTATION SUBMITTED 2022

AALBORG UNIVERSITY
DENMARK

Thermal conductivity of glasses: A structural point of view

PhD Thesis

Søren Strandskov Sørensen

Aalborg University
Department of Chemistry and Bioscience
Fredrik Bajers Vej 7H
DK-9220 Aalborg

Dissertation submitted: August 31st, 2022

PhD supervisor: Professor Morten Mattrup Smedskjær
Aalborg University

PhD committee: Associate Professor Casper Steinmann (chair)
Aalborg University, Denmark

Professor Benoit Rufflé
University of Montpellier, France

Professor Philip Stephen Salmon
University of Bath, United Kingdom

PhD Series: Faculty of Engineering and Science, Aalborg University

Department: Department of Chemistry and Bioscience

ISSN (online): 2446-1636
ISBN (online): 978-87-7573-838-0

Published by:
Aalborg University Press
Kroghstræde 3
DK – 9220 Aalborg Ø
Phone: +45 99407140
aauf@forlag.aau.dk
forlag.aau.dk

Printed in Denmark by Stibo Complete, 2022

English summary

Oxide glasses play a vital role in modern day life with applications within architecture, screen technologies, communications technologies, domestic and technical insulation materials, among many other uses. For many of these applications, structure-property correlations are well-studied. However, some properties remain much less explored - one such property of oxide glasses is thermal conductivity, despite its relevance for, e.g., insulation materials and for controlling thermal shock resistance. The aim of this thesis is thus to understand and develop such structure-thermal conductivity correlations in oxide glass systems

First, a variety of oxide glasses were studied experimentally in the lithium germanate and borosilicate glass families. These were chosen due to their inherent structural anomalies when adding network modifiers and/or changing the network former ratio. As such, they served as a means to deduce the correlations of composition and structure separately. This was used to showcase how two different contributions to thermal conductivity exist; one contribution dependent on composition, density, and sound speed from so-called *diffusive* vibrations. This contribution is possible to estimate through a simple semi-empirical model; and another contribution dependent on structure, namely, *volumetric constraint density*. This latter contribution is argued to stem from *propagative* vibrations. Intriguingly, it was found that the structure dependent contribution to thermal conductivity rises linearly with the volumetric constraint density for a number of modified oxide glass families - however, even though all correlations increased with increasing constraint density, the correlations varied significantly between glass families.

Second, the effect of pressure on thermal conductivity was studied in both an experimental series of hot-compressed borosilicate glasses and in a compressed simulated $30CaO\text{-}10Al_2O_3\text{-}60SiO_2$ glass. While the thermal conductivity in the borosilicates were shown to be described by the same two-contribution model as for other oxide glasses, the changes of thermal conductivity with compression was not directly explainable by a simple structural metric. As such, the changes are, at least partially, governed by structural changes of the medium-range order structure. For the calcium aluminosilicate glass, a detailed simulation of

thermal diffusivity and conductivity was conducted up to 100 GPa of pressure. It was revealed how thermal diffusivity and the amount of diffusive and propagative vibrations were significantly enhanced with increasing pressure, resulting in a large increase in thermal conductivity with increasing pressure. For more, an intriguing coupling between thermal conductivity and the Debye frequency as well as the so-called *boson peak* was found.

The outcomes of the present thesis is a deepened understanding of thermal conductivity beyond the most compositionally simple oxide glasses and a set of design criteria for manipulating thermal conductivity in this glass family. Specifically, to maximize thermal conductivity one must search for glasses of low molecular weight oxides and high rigidity, i.e., a high number of constraints per unit volume. Additionally, it was found how one may use post treatment methods to alter thermal conductivity in these systems. Ultimately, this work should be seen as the first step towards a more comprehensive understanding of the structure-thermal conductivity correlations and model-building in the oxide glass family. Something which may significantly affect the performance of numerous glass products and enhance the understanding of the physics governing heat transfer in complex amorphous systems.

Dansk resumé

Oxidglas spiller en central rolle i den moderne tidsalder med anvendelser indenfor arkitektur, skærmteknologier, kommunikation, isoleringsmaterialer, m.fl. For mange af disse anvendelser er struktur-egenskab sammenhænge velstuderende, mens de for visse egenskaber er langt mindre forstået - en sådan dårligt forstået egenskab er termisk ledningsevne, på trods af dens relevans for f.eks. isoleringsmaterialer og som en vigtig parameter i kontrollen af termisk chok. Målet med denne afhandling er at forstå og udvikle sådanne sammenhænge mellem struktur og termisk ledningsevne i oxidglas.

Først blev to serier af hhv. lithium germanat og borosilikat glas studeret eksperimentelt. Disse blev udvalgt grundet deres anomale ændring af koordinationstal med ændringer i hhv. modificerende oxid og netværksdanner for på den måde at kunne adskille bidrag fra struktur og komposition til termisk ledningsevne. Ud fra studier af disse blev det vist, at der kan udledes to forskellige bidrag til den termiske ledningsevne i oxidglas; et bidrag, som afhænger af glassets komposition, densitet og lydhastighed fra *diffusive* vibrationer. Dette bidrag kan estimeres med en simpel semiempirisk model; og et andet bidrag med en stærk afhængighed til struktur, nærmere betegnet mængden af atomare *begrænsninger* per volumen. Dette bidrag kommer fra såkaldte *udbredende* vibrationer. Det blev fundet, at det strukturafhængige bidrag til termisk ledningsevne havde en positiv lineær tendens med antallet af atomare begrænsninger per volumen for en række modificerede oxidglas. Imidlertid så selvom alle lineære tendenser var stigende med stigende antal af atomare begrænsninger per volumen, så varierede korrelationerne kraftigt mellem glasfamilier.

Dernæst blev effekten af tryk på termisk ledningsevne studeret eksperimentelt i en serie af højtryksbehandlede borosilikat glas og i et simuleret 30CaO-10Al_2O_3-60SiO_2 glas under tryk. Mens den termiske ledningsevne i borosilikatglassene blev fundet til at være velbeskrevet af to-bidrags modellen var det ikke muligt at korrelere de fundne ændringer med nogle simple strukturelle parametre. På denne baggrund blev det fundet, at den termiske ledningsevne, i hvert fald delvist, er styret af glassets mellemrækkende orden. Det studerede calcium aluminosilikat glas blev trykket med op til 100 GPa i molekylær dynamiske simuleringer. Fra disse blev det fundet, at den termiske diffusivitet

for højfrekvente vibrationer samt andelen af ikke-lokaliserede vibrationer steg kraftigt med stigende tryk. Dette medførte en kraftig stigning i den termiske ledningsevne som funktion af trykket. Ydermere blev der fundet interessante koblinger mellem termisk ledningsevne og Debye frekvensen samt den såkaldte *boson top*.

Resultaterne af denne afhandling er en dybere forståelse for den termiske ledningsevne af komplekse glas bestående af blandinger af oxider samt et sæt retningslinjer til at designe oxidglas med høj eller lav varmeledningsevne. Specifikt for at maksimere den termiske ledningsevne skal man søge glas med oxider af lav molarmasse og høj rigiditet, dvs. mange atomare begrænsninger per volumen. Derudover blev det fundet, at efterbehandlinger med f.eks. tryk også kan benyttes til at ændre den termiske ledningsevne i disse systemer. Endelig skal denne afhandling ses som det første skridt mod en mere dybdegående forståelse af struktur-ledningsevne sammenhænge og en egentlig model for termisk ledningsevne i et væld af oxidglas. Dette har potentiale til at forbedre egenskaberne af et væld af glasprodukter og forbedre forståelsen af den fysik, der styrer varmeoverførsel i komplekse amorfe systemer.

Acknowledgements

The submission of this thesis marks the end of my PhD journey. Albeit having faced a pandemic, I can honestly say that it has been an amazing trip both personally and academically. Naturally, I have been far from alone through my studies and therefore, I wish to thank a number of people.

First, my supervisor Professor Morten M. Smedskjær, who has been an always supportive and constructive aid in teaching me academia from the inside. Your supervision has pushed the limits of my abilities.

Second, I would like to thank the collaborators which have aided me throughout my PhD study: Hicham Johra, Christophe A. N. Biscio, Lisbeth Fajstrup, Lars R. Jensen, Esben Skovsen, Pawel P. Cielecki, Mathieu Bauchy, John C. Mauro, Kuo-Hao Lee, Randall E. Youngman, Stephan L. Logunov, Michał Boćkowski, and Sylwester J. Rzoska.

Next, I sincerely wish to thank my current and previous local colleagues and collaborators at the Department in Aalborg. Aamer, Ang, Anne, Anne-Sophie, Ayoub, Chao, Chengwei, Daming, Elsebeth, Jiajia, Johan, Kacper, Lisbeth, Luna, Malwina, Martin, Mette, Michelle, Mikkel, Naia, Pengfei, Peter, Qi, Rasmus, Rasmus, Rasmus, Sheng, Søren, Søren, Tao, Theany, Tobias, Wei, Wei, Xiangting, Yongbao, Yuanzheng, Zhencai, Zhimin, the others in the Section, and those that I must certainly forgot!

Last, but not least, I wish to thank my family: My wife, Nickie; kids, Felix and Silke; my parents; brother; grandparents; and in-laws for always believing in me and for their endless support.

Søren S. Sørensen

Søren Strandskov Sørensen
Aalborg University, August 31, 2022

Contents

Chapter 1

Introduction

1.1 Background

Glassy materials have been an irreplaceable part of the world for millennia [1]. From the usage of natural glasses as weapons and jewellery, glass has today been incorporated as an advanced technology and sees wide usage within materials science and engineering [1]. Its broad usage is greatly linked to a number of advantageous design parameters, e.g., oxide glasses generally (but not always) feature; i) great shapeability; ii) high chemical and mechanical durability, and iii) transparency [1–3]. While several other glass families exist, oxide glasses comprise the majority of produced glass, likely due to its chemical inertness, great transparency, and low cost, making it optimal for use in windowpanes and screen applications. Yet, even though silicate-based glasses see the largest bulk usage within windows, the use of oxide glasses in advanced technological applications continues to expand. This includes applications within glass fiber technologies for ultra-fast data transfer [4, 5], screen applications with highly crack resistant glasses [6], as parts in semiconductor devices [7], among many other uses [4, 8]. As such, the engineering of glass properties is a cornerstone of modern glass technology.

Now, while the engineering of glasses has traditionally been a trial-and-error process, the inconceivable amount of possible glass compositions make this process highly ineffective. As such, another approach to optimize glass properties is to understand the correlations between glass properties and the underlying glass structure [9]. This is a task of significant challenges, especially due to how the glass structure lacks the symmetry found in crystals, deeming common structure solving methods worthless. However, successful structure-property models for predicting both thermodynamic and mechanical properties have been developed, e.g. based on traditional rigidity considerations from local metal-oxygen coordination numbers in the so-called topological constraint theory [10]. Yet, despite the interest of correlating structural parameters to

glass properties, some properties have been notoriously neglected - one such property is that of thermal conductivity. While the thermal conductivity of glasses has seen quite some interest in classical physics for especially its low-temperature anomalies [4], very limited interest has been given to it as an engineering parameter near room temperature. This may be showcased by noting how only 35 entries of thermal conductivity is given in the SciGlass database - for comparison, 3987 entries of density and 816 entries of Young's modulus are indexed!

As such, describing thermal conduction in glasses is a persistent problem in solid state physics and engineering primarily caused by the lack of long-range order structure in amorphous materials. While significant progress has been made in the last three decades, many questions remain largely unanswered - especially for structures extending beyond the simplest compositions. As such, while some measurements of thermal conductivity in oxide glasses exist in the literature, fundamental understanding of its relation to structure remains unclear. Solving this puzzle could enable glass materials with optimized heat conductive properties for, e.g., passive layers in with improved heat transfer in electronics [7] and improved thermoelectric modules [11].

1.2 Scope and Objectives

The aims of this thesis is to provide some of the first steps towards establishing a correlation between structure and thermal conductivity in glasses. This has been done by studying a range of systems with anomalous structural behavior and their thermal conductivity to ultimately couple these parameters. Moreover, focus has been to apply compression methods to study their effect on both structure and related thermal conductivity using both experiments and numerical methods. This is done to induce structural changes without changing the composition. Apart from the work on structure-property correlations, some work has also been devoted to the development of new methods for structural characterization based on topological data analysis. In summary, the thesis will aim for elucidating answers for the following working questions:

- How may one characterize amorphous structure beyond the short-range order?
- How may one quantitatively describe medium-range order structure from simulations?
- How does chemical composition impact thermal conductivity in glasses?
- What is the effect of pressure on glass structure and thermal conductivity?
- Is it possible to correlate structural models to thermal conductivity in glassy systems?

- Is the thermal conductivity in glasses mainly governed by short- or medium-range order?

While a thorough understanding of the above questions will rather require a career than a single thesis, the current thesis aims to provide some of the initial steps in answering these fundamental and poorly understood correlations, with particular emphasis on the oxide glass family.

1.3 Thesis content

The main body of this thesis consist of the following papers and manuscripts prepared following my Master's defense in the Integrated PhD Programme (i.e. half time PhD student from August 2018 to August 2020 and full time PhD student from August 2020 to August 2022). The papers may be found separately in the Papers part of this thesis.

Paper I T. Du[1], S. S. Sørensen[1], T. To[1], M. M. Smedskjær, "Oxide glasses under pressure: Recent insights from experiments and simulations", *Journal of Applied Physics*, vol. 131, pp. 170901, 2022.

Paper II S. S. Sørensen, T. Du, C. A. N. Biscio, L. Fajstrup, M. M. Smedskjær, "Persistent Homology: A Tool to Understand Medium-Range Order Glass Structure", *Journal of Non-Crystalline Solids X*, In revision.

Paper III S. S. Sørensen, M. S. Bødker, H. Johra, R. E. Youngman, S. Logunov, M. Bockowski, S. J. Rzoska, J. C. Mauro, M. M. Smedskjær, "Thermal conductivity of densified borosilicate glasses", *Journal of Non-Crystalline Solids*, vol. 557, pp. 120644, 2021.

Paper IV S. S. Sørensen, T. To, J. F. S. Christensen, H. Johra, M. M. Smedskjær, "Impact of network topology on the thermal and mechanical properties of lithium germanate glasses", *Journal of the American Ceramic Society*, vol. 105, pp. 977, 2022.

Paper V S. S. Sørensen, P. P. Cielecki, H. Johra, M. Bockowski, E. Skovsen, Y. Yue, M. M. Smedskjær, "Thermal conduction in a densified oxide glass: Insights from lattice dynamics", *Materials Today Communications*, vol. 32, pp. 104160, 2022.

As the works published during the first part of the integrated PhD programme has been defended as part of my Master's Thesis (September 2018 to August 2020) it is not directly included in the present thesis. However, some of these

[1]Equal contribution

works will see continuous referencing as Refs. [12–15].

Apart from the above works, several contributions have been made to other published works. A full publication list (including the papers stated above) is found on page 73.

Chapter 2

Glass Structure

While the main constituents (and hence composition) of oxide glasses have been known for millennia, the resulting structural arrangement continues to provide significant trouble to grasp for scientists. In this chapter, the fundamentals and recent advances in understanding of oxide glass structure will be discussed. For more, suitable models for describing glass structure will be introduced.

2.1 Structure of simple oxides

Crystalline materials are characterized by the possession of long-range order by the replication of a single unit of structure, the so-called *unit cell* [16]. This long-range order is basis for the whole scientific field of crystallography, that is, the solving of atomic positions within crystal lattices [17]. As such, it may not be surprising that it was a crystallographer who made some of the most important contributions to the understanding of glass structure.

Based on the knowledge of crystal structures in various metal oxide systems, Zachariasen was the first to put a number of empirical rules of what constitutes oxide glass structure [18]. He summarized some guidelines for what is ideal for optimizing glass-formation. Namely that (quoted from Ref. [18]) *an oxide glass may be formed*:

- *if the sample contains a high percentage of cations which are surrounded by oxygen tetrahedra or by oxygen triangles;*
- *if these tetrahedra or triangles share only corners with each other and;*
- *if some oxygen atoms are linked to only two such cations and do not form further bonds with any other cations.*

Additionally, he deduced how glasses have a lack of symmetry and hence how a glass would constitute an *infinitely large unit cell* where the local geometry would mimic that of the crystal yet that each atom would be structurally

unique. For oxide glasses, the two most archetypical oxide glass formers are likely SiO_2 and B_2O_3. Their fundamental metal-oxygen building block of tetrahedral and triangular characters, respectively, are presented in Figures 2.1a-b.

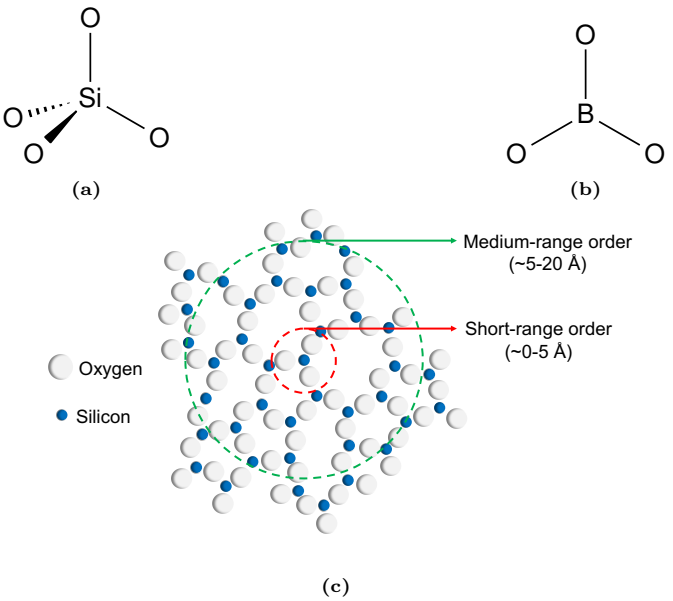

Fig. 2.1: Fundamental tetrahedral and triangular building blocks in (a) SiO_2 and (b) B_2O_3 glass, respectively. (c) Planar sketch of the SiO_2 glass structure (where one oxygen is omitted for clarity) with approximate depictions of the short- and medium-range order domains. Figure (c) is reprinted from Paper II.

While Zachariasen clearly depicted the full amorphicity and resulting lack of long-range order, as well as the similarity between the local structure (i.e., the short-range order) in the crystal and glass, it is essential to bear in mind how some structural order beyond the short-range order, but before full randomness, is maintained. This structural regime is typically coined *medium-range order* (MRO). While it is generally well-established that this structural regime exists, it is much harder to characterize compared to short-range order (SRO). Generally, MRO structure is believed to extend from around 5 to 20 Å [19] although the cutoff value is very poorly defined. Beyond the MRO, no order exists and the material is thus amorphous. This perception of Zachariasen is termed the *random network model* [18]. While this model stands as perhaps the singlemost important perception of glass structure, it mainly applies to pure oxide glass formers. This contrasts with most actual oxide glasses which incorporate multiple oxide types - even those which are not good glass formers themselves - this is commonly alkaline, alkaline earth, and transition metal

oxides [2]. These additions give rise to new chemical and physical properties as well as new structure.

2.2 Structural changes with composition

2.2.1 Oxide classification

When mixing different oxides to form a homogeneous phase, a variety of structural features arise. These changes are greatly linked to the type of oxide added - as such, it is very convenient to have a means of grouping these compounds. Dietzel provided a method for such grouping by introducing the *field strength* (FS) of oxide materials [20], i.e.,

$$FS = \frac{Z_c}{a^2}, \tag{2.1}$$

where Z_c is the cation charge, and a is the separation of the oxygen and cation ($a = r_{\text{oxygen}} + r_{\text{cation}}$). This eventually provides a measure of the bonding type of the bond formed between the cation and oxygen (higher FS, higher covalency). Now, according to Dietzel, three groups may be distinguished, i.e. network modifiers ($FS \approx 0.1 - 0.5$), network intermediates ($FS \approx 0.5 - 1.2$), and network formers ($FS > 1.2$). Network formers are what is described in Zachariasen's model and tend to form bonds with oxygen of a large covalent character. This stands in contrast to network modifiers which form ionic bonds with oxygens with a generally larger bond distance and consequently a higher coordination number (also explaining why they are poor glass formers in their pure form). In between these two extremes, intermediates have the possibility to act both as network formers and modifiers, depending on the nearby chemical environment [2]. A compilation of the most common oxides and their FS is given in Table 2.1.

Table 2.1: List of some of the most common ions found in oxide glasses and their associated field strengths. List reproduced after Ref. [20].

Ion	Coordination	Charge	Ionic distance (Å)	Field strength (Å^{-2})
Li^+	6	1	0.210	0.23
Na^+	6	1	0.230	0.19
K^+	8	1	0.277	0.13
Mg^{2+}	6	2	0.210	0.45
Ca^{2+}	8	2	0.248	0.33
Sr^{2+}	8	2	0.269	0.28
Al^{3+}	6	3	0.189	0.84
	4	3	0.177	0.96
B^{3+}	3	3	0.150	1.34
Si^{4+}	4	4	0.160	1.57

2.2.2 Modified oxide glasses

Practically, the majority of glasses are mixtures of different oxides including network formers, intermediates, and modifiers, and, as such, a very diverse structure is obtained in these glasses. In the 1930's, Warren and Biscoe [21] studied one of the most archetypical modified oxide glasses, namely sodium silicates ($x\mathrm{Na_2O}$-$(100-x)\mathrm{SiO_2}$), using X-ray diffraction. From their studies, they proposed how the structural character of the glass changed when adding modifiers to network formers. Specifically, they found that modifier ions (in this case $\mathrm{Na^+}$) will break up the polymerized network (Si-O-Si), creating so-called *non-bridging oxygens* (Si-$\mathrm{O^-}$). This perception has later been found to also be applicable for other network modifiers. A schematic of this structural perception is presented in Figure 2.2a.

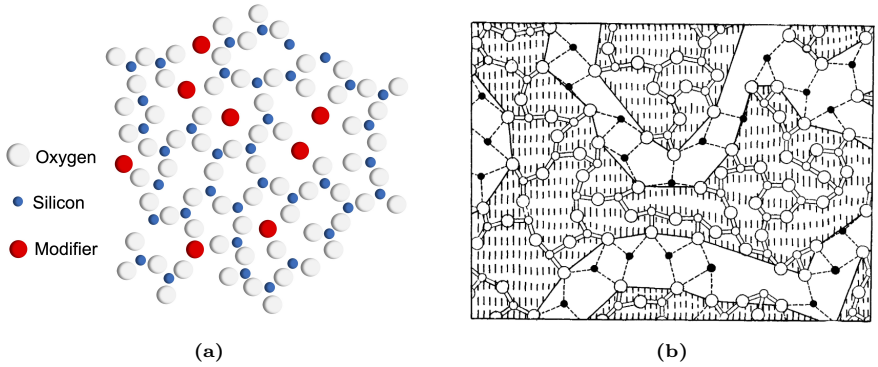

Fig. 2.2: (a) Structural perception of how modifier ions may disrupt the fully polymerized glassy network by creating non-bridging oxygens and larger ring-type structures. (b) Depiction of how modifier atoms (black dots) place themselves in tunnel-like structures inside the polymerized glass matrix as suggested in the *modified random network model*. Figure (b) is reprinted from Greaves, *J. Non-Cryst. Solids*, **71**, 203 (1985) [22]. Copyright 1985 Elsevier.

While this result has laid the foundation for the understanding of both structure and structure-property correlations in numerous oxide glasses, the understanding has been further deepened. Based on extended X-ray absorption fine structure (EXAFS) measurements, Greaves [22] introduced the *modified random network model*. Here, EXAFS revealed how modifying cations have a non-random order, at least in vicinity of the oxygen atoms [23]. For more, Greaves [22] depicted how modifier cations arrange in tunnel-like structures in the network former matrix. Later, this perception has come to be the dominant belief, yet with the note that the tunnel-like structure are rather dynamic than static and best practically envisioned by following the diffusion of modifier cations in the glass, e.g., in simulation studies. A depiction of the tunnel-like structure in a simple modified oxide glass is presented in Figure 2.2b.

2.2.3 Structural anomalies

Now, while the pure metal oxides all have well-defined cation coordination numbers (CNs), adding other oxides (both formers, intermediates, and modifiers) will in some cases dramatically change the cation coordination. As examples, Si, B, and Ge in their pure oxide forms have cation CNs of 4, 3, and 4, respectively. However, addition of network modifiers will have very different effects. i) For SiO_2, adding modifiers will generally not change the Si CN, but depolymerize the overall network by producing non-bridging oxygens [2]. However, the most notable exception is how adding pure P_2O_5 will induce the presence of six-coordinated Si [24], something which is otherwise mainly seen in high-pressure polymorphs [25]; ii) For B_2O_3, adding network modifiers will, at lower modifier concentrations, induce the transformation from three- to four-coordinated boron and thus a strengthening of the overall network [26]. This transform is termed the *boron anomaly*. At further modifier addition, the coordination number change will revert back to a coordination number of 3, yet now with non-bridging instead of bridging oxygens; Finally, iii) upon modifier addition to GeO_2, Ge will also increase its coordination number from four to five and/or six (the specific change is under considerable debate, see Refs. [27–29]). At further modifier addition, the coordination number change of the cation will revert, but now with non-bridging instead of bridging oxygens attached to the cation polyhedra. These three situations are sketched in Figure 2.3.

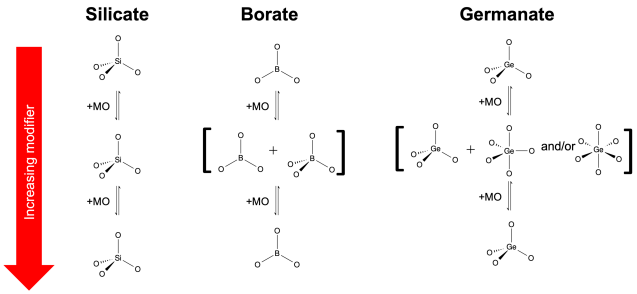

Fig. 2.3: Sketch of how silicate, borate, and germanate polyhedra change coordination number upon increasing modifier concentration. Depictions of bridging/non-bridging oxygens are omitted for clarity.

These structural changes significantly affect the properties of the glasses. That is, silicates will tend to see a decrease in structural polymerization with increasing modifier concentration while borates and germanates will *increase* their polymerization. Practically, this affects many properties, perhaps most notably the glass transition temperature (T_g). The T_g will generally follow

the degree of polymerization and thus for silicates, the T_g will often decrease for increasing modifier content while the T_g of borates and germanates will (up to a given concentration) increase due to the increasing polymerization. While this is a rule of thumb it will highly depend on the modifier, with high FS modifiers (typically high charge, low Z cations) deviating more from the above statements [13]. An example of the correlation between FS and T_g for a series of 20MO-80B_2O_3 glasses (with M being either one or two metal cations) with alkali and alkaline earth metal oxide modifiers from our earlier work as presented in Figure 2.4.

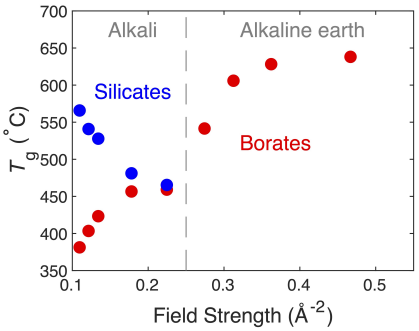

Fig. 2.4: The glass transition temperature (T_g) of multiple modified silicate and borate glasses with compositions of 20MO-80SiO_2 and 20MO-80B_2O_3 where M is one or two metal ion(s). The field strengths correspond to (from left to right) Cs, Rb, K, Na, Li, Ba, Sr, Ca, and Mg, respectively. Figure is reprinted from Sørensen *et al.*, *Appl. Phys. Lett.*, **117**, 031901 (2020) [13]. Copyright 2020 AIP Publishing.

While there exist more structural anomalies in glasses, the above examples are the most prominent and studied in the literature. As such, these are also the anomalies which will later be discussed in relation to their effect on heat transfer in these glass systems.

2.3 Structural changes with pressure

While many structural changes may be unveiled through compositional change, different kinds of treatments provide means of permanently modifying the glass structure without changing the composition. Several treatments enabling such changes rely on changing the pressure. Paper I of the present thesis presents a perspective article specifically devoted to describing the techniques involved in glass compression, the resulting structure and property changes, as well as the perspectives of the field.

The methods of applying pressure to modify glasses can mainly be divided into two groups, namely, cold- and hot compression. First, cold compression typically involves compressing a sample at room temperature using a uniaxial press or a diamond anvil cell (DAC), ideally creating uniaxial stress/strain or

isostatic stresses, respectively. At lower pressures (few GPa) this will usually only induce reversible deformations, but by increasing the pressure, permanent densification and structural changes will evolve [30]. Second, hot compression may involve several compression methods, but, as the name depicts, is performed at elevated temperatures, typically on the order of the glass transition temperature of the studied glass or even in the melt [31, 32]. For more, while both uniaxial presses and DACs may be used for hot compression experiments, it is often also performed using N_2 gas as the compression medium [31]. The latter limits the maximum pressure to few GPa, but ensures full isostaticity. While high temperature treatments will induce structural changes which, to some degree, mimic those of cold compression, permanent changes will usually appear at much lower pressures compared to cold compression [31, 33].

Structurally, the changes upon densification may be split into short- and medium-range order changes. For SRO, various coordination number changes are apparent upon compression very much depending on the glass type. For the three glass types studied here (SiO_2, GeO_2, B_2O_3), their pure forms see notable differences in their pressure response upon cold compression as compiled in Figure 2.5.

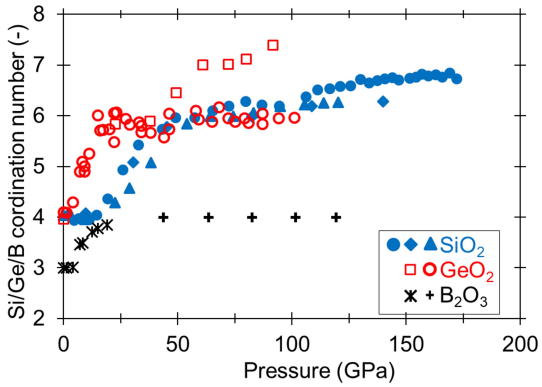

Fig. 2.5: Coordination number of Si, Ge, and B in SiO_2, GeO_2, and B_2O_3 under cold compression to megabar pressures. Data are collected from Refs [25, 34–39]. Figure is reprinted from Paper I.

Specifically, while GeO_2 and B_2O_3 see notable CN changes from 0 to 20 GPa (averagely from four to six and three to four, respectively), the pressure response of the SiO_2 CN (from four to six) is initiated at around 20 GPa and completes at around 50 GPa. Further increasing the cold compression pressure will not provide any changes to the CN of B_2O_3, but recent works [25, 35] have argued that both GeO_2 and SiO_2 see CN increases to above six in such pressure regime. However, other works [36] argue for less or no changes and, as such, complimentary measurements are needed to thoroughly determine the nature of this phenomena and to determine whether the proclaimed CN changes above six are indeed real. For hot compression studies, the pressure range is generally

more limited, but the same tendencies are apparent, that is, SiO_2 is less labile for CN changes than other oxides [31, 40].

At the medium-range order scale, changes are often way more complex to describe. Despite this, notable changes to many glass systems have been described in the literature. Generally, polymerization will increase upon increasing pressure as CNs increase. This is both true for the network former and modifier cations, yet also for the oxygens in the oxide glasses. As such, the average Q^n (that is, the number of bridging oxygens per network forming cation) will tend towards higher n for higher pressures [31]. Other experiments have found types of clustering in different oxide glasses, e.g., finding that three- and four-coordinated borons tend to cluster separately in modified borate glasses, yet that such clustering decreases upon increasing pressure [41]. Interestingly, such arguments of inhomogeneity have also been found to apply to pure oxides, e.g., SiO_2, yet here with a less clear specification of its structural origin [42–44]. Other common ways to characterize MRO rely on characterizing the ring-type structures found in oxides upon pressure addition. This is highly complex and will generally rely on the access to three-dimensional structural data, commonly acquired from structural refinement or pure simulation studies. Upon increasing pressure, ring sizes (typically counted as the number of network forming cations in the ring) tend to decrease, in agreement with the general idea of how the network compacts and increases its nearest neighbor count [45]. Recently, the idea of characterizing ring structure distributions directly through experimental data have been developed as the so-called RingFSDP method [46, 47]. This method relies on decomposing the so-called *first sharp diffraction peak* (FSDP) into contributions from different ring structures. The general idea of the RingFSDP method will be briefly introduced in Section 2.4.1. While this method is very new, it has only seen application to few glass compositions, but given the rather vast amount of experimentally available data, its application to many already tested glasses should be of great interest for providing new understanding in the pressure response of glasses.

2.4 Characterizing glass structure

Despite how Zachariasen did indeed grasp the oxide glass structure in a very meaningful manner, the available experimental techniques capable of confirming his ideas at the time of publication was, at best, limited. In fact, it is first within the last few decades experiments have provided direct visualized confirmation of the amorphous nature of the oxide glass structure from e.g., electron microscopy [48]. However, a number of other methods have provided invaluable information of both the short- and medium-range order glass structure. In the following section the fundamentals of a few of these methods will be introduced and the possible insight gained from them will be discussed.

2.4.1 Experiments

With regard to the importance of X-ray diffraction methods for studying crystals it may not be surprising how diffraction methods have been one of the most used methods for characterizing glass structure. For crystals, the repeating unit (i.e., the *unit cell*) governs the intense pattern observed in a diffraction experiment from crystalline materials through Bragg's law, i.e. [16],

$$2d\sin(\theta) = n\lambda, \tag{2.2}$$

where d is the interplanar spacing, θ is the angle between the incoming radiation and the crystallographic plane, and λ is the wavelength of the incoming radiation (typically in the X-ray range as its wavelength is equivalent to typical interplanar spacings). This equation relies on the crystal lattice and is thus not applicable to amorphous materials, including glasses. However, as it will be seen, glasses also feature characteristic scattering patterns when observed in a setup similar to that of crystal experiments, yet at a much smaller intensity. Fundamentally, this scattering pattern stems from the interatomic pair distances in the material. This correlation was discovered by Debye and compiled as the so-called *Debye scattering equation* [49, 50],

$$I(Q) = Nf^2 + f^2 \sum_n B_n \frac{\sin(Qr_n)}{Qr_n}, \tag{2.3}$$

where the intensity (I) at a given momentum transfer (Q), is given as a function of the number of atoms (N), the scattering factor (f), the number of atomic pairs B_n, and the interatomic pair distances (r_n). While a full derivation is beyond the scope of the current thesis, the biggest achievement of Eq. 2.3 is how one can relate atomic pair distances directly to a measurable quantity! After the introduction of Eq. 2.3, the equation was rewritten in a more convenient form [51], i.e.:

$$I(Q) = Nf^2\{1 + \int 4\pi r^2[\rho(r) - \rho_a]\frac{\sin(Qr)}{Qr}\mathrm{d}r\}, \tag{2.4}$$

where $\rho(r)$ and ρ_a are the density of atoms at r and on average, respectively. Importantly, the term $4\pi r^2\rho(r)$ represents the *radial distribution function* (RDF) which provides the direct real space information on the probability of finding an atom at a given separation [52]. Likely best noticed from Eq. 2.4, there exist a Fourier transform relation between the intensity observed experimentally from Q-space and to the real-space information of the RDF.

While Eqs. 2.3 and 2.4 are generally valid for a monatomic system, the majority of chemistry and physics is concerned with multiatom systems. The perhaps most common approach for overcoming this extension was developed based on the work of Faber and Ziman in the 1960's. The multiatom total structure factor may be expressed as a sum over all *partial* structure factors ($S_{ij}(Q)$) as [53],

$$S(Q) = \frac{\sum_{i,j=1}^{n} c_i c_j b_i b_j S_{ij}(Q)}{\left(\sum_{i=1}^{n} c_i b_i\right)^2}. \tag{2.5}$$

Here, each partial structure factor is directly linked to the partial radial distribution function ($g_{ij}(r)$) through,

$$S_{ij}(Q) = 1 + \rho_a \int_0^\infty 4\pi r^2 (g_{ij}(r) - 1) \frac{\sin(Qr)}{Qr} \mathrm{d}r \tag{2.6}$$

The partial radial distribution function compiles the pairwise distances encountered in the material for each atomic type. One may note the clear relation between Eqs. 2.4 and 2.6. Practically, one may often encounter the above equations and their results from several sources: i) From scattering experiments where one may measure the structure factor and then subsequently deduce the RDF, or; ii) from modelling, where one may directly get the pairwise distances and then transform into the structure factor (often with the objective to compare to experimental data). Both i) and ii) are performed by a Fourier transform of the RDF to/from the structure factor. An example of a structure factor ($S(Q)$) and the related radial distribution function ($g(r)$) of a simulated 30CaO-10$Al_2O_3$60SiO_2 glass from Paper V is presented in Figure 2.6 together with the typical naming of peaks in $S(Q)$ and the most ordered atomic correlations of the $g(r)$.

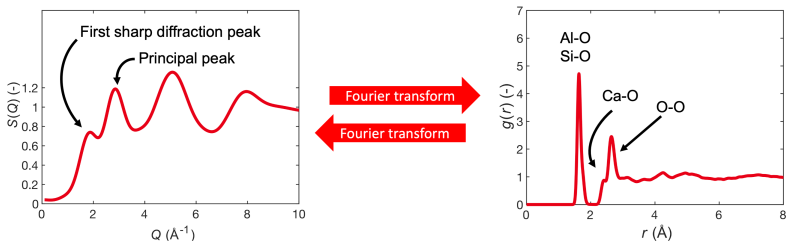

Fig. 2.6: (Left) Structure factor of an uncompressed simulated 30CaO-10$Al_2O_3$60SiO_2 with typical naming of the two peaks at the lowest values of momentum transfer and (right) its corresponding radial distribution function with depiction of the atomic correlations involved. Figure is adapted from Paper V.

The obtained data is in any case relevant for deeper analysis. As briefly discussed, atomic separations as well as coordination numbers are obtainable from the RDF. For the structure factor, direct structural interpretation is somewhat more difficult, however some methods for structural descriptors are used. Most notably is probably the use of the FSDP, that is, the peak at the lowest momentum transfer (Figure 2.6), often taken as a fingerprint of MRO structure. The value of Q is commonly transformed into a real-space metric through $Q = 2\pi d^{-1}$ (originating from the relation of momentum transfer and lattice spacing in a cubic crystal) [16]. This real space value is often argued to be

related to the rings in the glass structure [54] which creates *pseudo planes* of relatively regular separation. An adapted version of this approach is also the general idea of the RingFSDP method [46, 47]. A sketch of this is presented in Figure 2.7. As such, the Q-value associated with the FSDP is often reported, e.g., as a function of pressure to provide a means for describing MRO changes.

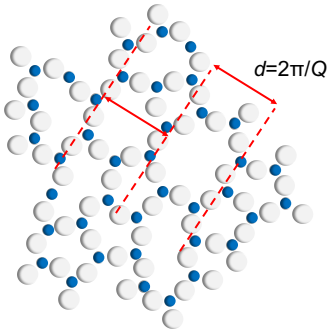

Fig. 2.7: Sketch of simplified SiO_2 structure and the perception of pseudo planes generated by the atomic rings. It is these planes which are often argued to represent the distances found in the first sharp diffraction peak (FSDP). Given how the FSDP is commonly appearing in the Q-range of 1-2 $Å^{-1}$, this roughly corresponds to pseudo plane distances of between 3 and 6 Å.

While diffraction measurements are often of great value due to their quantifiability and the ability to extract a lot of real space structural information, interpretation can in many cases be difficult, especially beyond the first coordination shell. For this, other experimental methods provide complimentary structural insight.

A group of markedly exploited methods are those in the family of spectroscopy. Within glass science, one of the most used methods is Nuclear Magnetic Resonance spectroscopy (NMR) [55, 56]. This method relies on measuring nonzero spin in atomic nuclei. Such spins are, e.g., apparent in ^{29}Si, B, ^{27}Al, and ^{17}O. Each unique NMR-active nucleus will have a resonance frequency (typically in the radio frequency spectrum) which may be measured. However, the resonance frequency is highly dependent on the local chemical environment. This is sometimes indicated by the *shielding* of a nucleus which is commonly quoted as a function of the local electron density [57]. While a thorough introduction to the NMR method is beyond the scope of this thesis, the main exploitation is how various chemical groups will have distinct resonance frequencies and thus serves as a fingerprint of its presence in the material. This is, for example, useful for the distinction and quantification of CN states in borate, silicate, and alumina containing glasses. This is showcased in Paper III which incorporates CN determination of boron from NMR measurements. Additionally, Q^n states are commonly derived from NMR experiments [56]. Apart from single-nucleus (1D) experiments, (e.g., 2D) corre-

lation experiments are one of the great advantages of NMR. Here, correlations between different chemical signals may be acquired to reveal whether they are in chemical proximity. This has, for example, been the main driving force to reveal the nature of how aluminium and various boron species place themselves in glass structure [56, 58]. While NMR has become one of the most important techniques for structural characterization in glass science, its main drawback is how only some isotopes are probeable. This problem is caused by how some elements have extremely low sensitivities, abundances, or zero spins (Ge has, e.g., only one NMR sensitive isotope of low sensitivity and abundance, making NMR an infeasible technique to study GeO_2 glasses) [56]. This may in some cases be solved by isotope enrichment, but this often comes at high cost. Generally, NMR is a unique technique within spectroscopy due to its reliance on the nucleus spin. Other common spectroscopic methods will typically rely on the vibrational characteristics of the studied material. This is the case for, e.g., infrared, Raman, and Brillouin spectroscopy which will be briefly introduced in the following.

To get an idea of the difference between the mentioned techniques, it is useful to have an understanding of what a vibration is. Here, the simplest models are based on linear chains of atoms. From a simple consideration of a two-atomic system in an infinite linear chain (top of Figure 2.8a) one may derive the related dispersion relation, i.e., the relation between wavelength and frequency [16, 59]. Notably, it will be found how the dispersion relation will feature two *branches*, namely an acoustic and an optical branch. These are characterized by being in- and out-of-phase vibrations, respectively. In the low wavevector limit (i.e., at long wavelengths), the acoustic branch approaches zero frequency while the optical branch approaches a finite frequency. These collective vibrations in the chain is the basic concept of *phonons*. The theory may be extended to 3D materials and generally for a crystalline material, the number of branches in the dispersion relation equals $3N$ (with N being the number of atoms in the unit cell). From these, three branches are acoustic and the remaining are optical. For any amorphous material, the concept of a unit cell effectively breaks down, and this will in fact also break down the concept of the dispersion relation. However, the existence of vibrations is obviously still present, but vibrations may not be characterized explicitly as acoustic or optical. Yet, similar to the crystal, each vibration will still be associated with a given energy which will induce its excitation. This may happen through electromagnetic radiation. In that sense, the material will absorb light with energy corresponding to a given vibrational feature. This is the principle of infrared (IR) spectroscopy (Figure 2.8b) where a range of frequencies irradiate a sample before the intensity of the outcoming radiation is measured [52].

Here, each absorption frequency will correspond to a unique vibration. By comparing with, e.g., crystalline materials from which the structure is known, or theoretical calculations, it is often possible to provide structural assignments to found absorption bands [59]. While IR is perhaps the most common spectroscopic technique, only some vibrational modes are accessible. As such, other

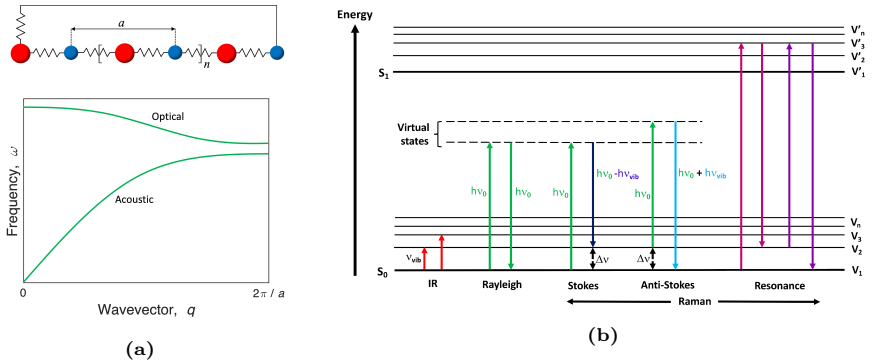

Fig. 2.8: Schematics of (a) the diatomic linear chain with periodic boundary conditions and the corresponding dispersion relation showing one acoustic and one optical phonon branch and; (b) the vibrational and electronic energy levels and the corresponding absorption and scattering processes producing the signals and IR and Raman spectroscopy. Figure (b) is reprinted from Geraldes, *Molecules*, **25**, 5547 (2020) [60] under an Open Access License.

techniques are highly useful. Specifically, scattering techniques have been the method of choice. One may imagine a number of possible outcomes of scattering when irradiating a sample. These are depicted in Figure 2.8b. First, the material may be excited to a *virtual state* which will quickly relax towards one of the lower energy vibrational states with the release of a new photon. If the incoming and outgoing photons are of equal energy the scattering is elastic. This is, by far, the most common phenomenon and is termed Rayleigh scattering. However, this provides no information on the vibrations in the studied material. Now, instead of Rayleigh scattering, it is found that some photons are *inelastically* scattered, i.e., the energy of the in- and outcoming photons are not equal. This is the so-called Stokes shift. When the energy is lower in the out- than the ingoing photon it is called a Stokes process, while the increase in energy is termed to be Anti-Stokes [52]. Eventually, this will enable the plot of a spectrum with intensities corresponding to the presence of vibrational modes. This principle is exploited in both, Raman and Brillouin spectroscopy. The fundamental difference between these two techniques is which frequency regions (and thus phonons) are studied. Low and high frequency modes, and thus acoustical and optical phonons, are studied by Brillouin and Raman spectroscopy, respectively [52, 61]. As such, Brillouin may be exploited to show largely collective in-phase vibrations and ultimately derive the sound speed and elastic characteristics of a material. This is done in Paper III for a series of soda lime borosilicate glasses to determine their transversal and longitudinal sound speeds and related elastic moduli. In comparison, Raman spectroscopy will probe the optical phonons and thus rather provide a fingerprint of local structural features and, as such, Raman is the prevalent method for characterizing structure. While more experimental methods exist, the above mentioned are those most commonly found in the literature and which has served as the

basis for the current understanding of glass structure within all glass families.

2.4.2 Topological constraint theory

Even though experimental observation is needed to confirm predictions and confirm theories, models of structural behavior is highly useful for coupling to properties and eventually for designing glasses of pre-engineered properties.

For this purpose, a number of models exist. One of the most successful models which has been developed throughout the last 50 years is that of topological constraint theory (TCT) originally developed by Philips and Thorpe [62, 63]. In TCT, each atom is taken as a *node*. Now, the bonds which exist between the atoms in the material is mimicked by a truss which *constrain* the atom. As such, this fixation is termed a *constraint*. Two types of constraints exist, namely linear and angular constraints. Linear constraints represents the ability of the bond to stretch while angular constraints describe the fixation of the angle between two bonds. Generally, the number of atomic constraints (n) have a simple relation with the average CN of the system ($\langle r \rangle$) [10].

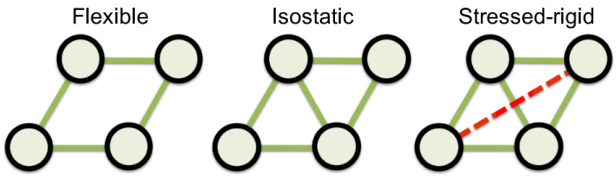

Fig. 2.9: Structural sketches of (left) flexible/underconstrained, (middle) isostatic, and (right) rigid-stressed structures. Figure is reprinted from Bauchy, *Comp. Mat. Sci.*, **159**, 95 (2019) [64]. Copyright 2019 Elsevier

Now, it is generally argued that there exist three regimes of rigidity when comparing n with the three degrees of freedom ($DOF = 3$) of a system (Figure 2.9). First, $DOF > n \rightarrow n < 3$. This regime is termed as the structure being *floppy*, *flexible*, or *underconstrained*. Here, the material will show little resistance to stress, often leading to easy crystallization and low glass-forming ability. Second, $DOF = n \rightarrow n = 3$. This appears at $\langle r \rangle = 2.4$ which is the *isostatic* state. This is believed to be the case of maximum glass-forming ability and it is believed that the isostatic state is greatly related to so-called *intermediate phase* glasses which are stress free and have been argued to feature a variety of special features [65]; Finally, $DOF < n \rightarrow n > 3$. This regime is termed *stressed-rigid* or *overconstrained* and will correspond to a solid material, yet with a greater tendency for crystallization compared to the isostatic state. The three states are sketched in Figure 2.9. While TCT was originally developed for chalcogenides (due to the ease of calculating their average coordination numbers) [10, 62, 63], it has later been adopted to oxides. Currently, there exist a number of TCT models for, e.g., modified borates [66, 67], borosilicates [68], aluminoborosilicates [69], phosphates [70], borophosphates [71], phosphosili-

cates [72], and germanates [28], some of which will be highlighted later in the present thesis as part of Papers III and IV.

2.4.3 Computational methods of making and characterizing glass structure

Analytical models are in many cases very useful but will often lack predictability beyond for what it is specifically made for. In such cases, actual atomic models are often of great usage combined with proper tools for analyzing the obtained structure. While a number of methods for doing this exist, this thesis will introduce only one of them which may be exploited to enhance the knowledge of glass structure.

Atomistic simulations

The perhaps most popular way of obtaining amorphous structures in computer simulations is through the so-called *molecular dynamics* (MD) technique. Here, forces are calculated from a *force field* or from quantum mechanics. With the availability of atomic forces, the actual movement (and dynamics!) of an atomic system may be simulated. This simply relies on Newton's second law of motion, $\bar{F} = m\bar{a}$, where $\bar{F}$ is the force, m is the atomic mass, and $\bar{a}$ is the acceleration. Now, through the assumption of a timestep (Δt, typically on the order of 1 fs), dynamics may be initiated using the Verlet algorithm [73], i.e.:

$$\bar{r}(t + \Delta t) = 2\bar{r}(t) + \bar{a}(t)\Delta t^2 - \bar{r}(t - \Delta t) + \mathcal{O}(\Delta t^4), \tag{2.7}$$

where $\bar{r}$ is the atomic position. After the first step, a new force may be calculated and the cycle may be repeated. Generally, the cycle performed in MD simulations is sketched in Figure 2.10.

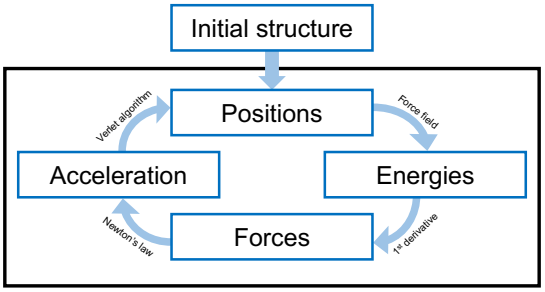

Fig. 2.10: Fundamental algorithm of molecular dynamics methods.

The functional used for calculating the force and relating acceleration may range from simple pairwise functionals to including a variety of complex multiatom correlations and/or bond angle restrictions. A number of force fields have been specially designed to replicate glass structure and properties [74, 75].

For making glasses, the most common approach is to start with a crystalline or random configuration. Then, the molten state is simulated for some time to equilibrate the liquid before initiating cooling into the glassy state. While the simulation size and time is usually on the scale of thousands of atoms and several nanoseconds for classical MD, quantum mechanical MD is usually limited to few hundred atoms and some hundred picoseconds of simulation time [75, 76]. This makes the cooling rates from the melt to the glassy state extreme compared to experiments. However, for classical force fields, the parameters are usually parameterized to account for this difference to obtain a realistic structure [77]. While some highly successful parameterizations exist for specific glass compositions [75], the tranferability to other glass types is often limited, yet the flexibility of the MD method is a great advantage. As such, MD allows for performing a variety of studies including those purely dedicated to understanding structure, but given the access to atomic forces, studies of mechanical and thermodynamical properties are possible, as well as atomic scale resolution even under dynamic conditions or conditions for which the force field was not specifically made. This is the vast advantage of the MD method. However, the possibility to perform a calculation does not ensure its reliability. As such, one should be careful to evaluate the results gained from MD simulations against experimental observation before considering it reliable. This problem even comes down to individual property-predictions of force fields where some properties may be well-predicted while others are simultaneously fully unreliable.

Persistent homology

While methods like MD simulations and other structure generating techniques may provide atomic resolution structures, the goal is not only to obtain the atomic structure, but also provide meaningful characterization of it. While a large number of possibilities for characterization exists (e.g., by applying methods also directly comparable with experiments like the scattering functions described in Section 2.4.1), dedicated methods for describing atomic positions is also of great use. While a thorough description of multiple methods is beyond the scope of the thesis, some work has been devoted to describing and developing one such method, namely that of *persistent homology* (PH). This method is a sub-method within topological data analysis and will be introduced here. The reader may note how Paper II included in this thesis is a dedicated introduction and mini review of the current state of the use of persistent homology in glass science. For more, the author has also previously actively used PH for structural characterization in simulated oxide glasses, see e.g. Ref. [14].

In PH, the basic principle relies on having access to all atomic coordinates. Now, each atom is replaced by a ball of a predetermined radius (which may vary between atoms). This radius may be either zero or nonzero, but has commonly been chosen to mimic the ionic radius of the given element through simple evaluation of radial distribution functions [14, 78–80]. Now, in PH, the

balls are allowed to grow by increasing their radii. This growth of radii is in PH denoted as increasing *time*, despite it having no relation to the physical meaning of time. With the increasing radii, balls will continuously touch. We will here provide examples of how PH groups the different cases in the case of a three-dimensional starting structure, that is in so-called 0, 1, and 2 dimensional PH. For 0D PH, connected components are studied. Here, persistence features are *born* at the point of zero time (i.e., at the initial radius) and *die* when two balls touch as shown in Figure 2.11a. This allows the plotting of a simple scatter plot with the birth and death time, a so-called *persistence diagram* (PD).

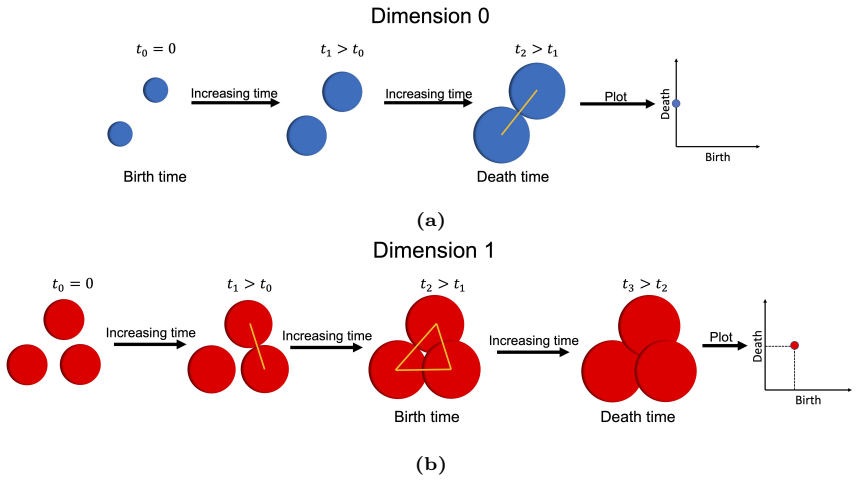

Fig. 2.11: Sketches of the birth and death times as well as persistence diagrams of dimension (a) 0 and (b) 1 persistent homology. t denotes time. Figure (b) is adapted from Paper II

For 1D PH, ring-type structures (often denoted as *loops*) are studied. A loop is born when a number of connected components form a closed ring. By increasing the radii further, the radii will at some point fully overlap the area of the loop. The exact time at which this happens is denoted as the death time of 1D PH features. An example of the birth and death of a 3 atom loop as well as the corresponding PD is presented in Figure 2.11b. Larger loops are also commonly found in PH analysis of glass structure [14, 79]. Finally, 2D PH studies *voids* in the atomic structure. That is, when dead loops fully enclose a structural void, the void will be born. With the increasing radii, the void will at some point be filled completely by the growing radii. At the point of complete filling, the death time is reached. While the use of PH is still in its infancy for the study of glass structure some works on, e.g., silicate glasses have been performed [14, 34, 79]. An example of the PD of a $20Na_2O$-$80SiO_2$ glass and the underlying loops is presented in Figure 2.12.

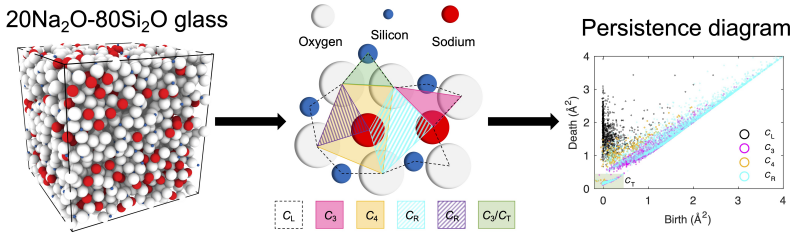

Fig. 2.12: (Left) Simulated structure of a $20Na_2O$-$80SiO_2$ glass and its (middle) corresponding loops and (right) persistence diagram of dimension 1. Figure is reprinted from Sørensen *et al.*, *Sci. Adv.*, **6**, eabc2320 (2020) [14] under an Open Access license.

It is noteworthy how PH has so far largely been used for characterizing glass structure under various compositions and conditions, yet that the use of PH as a model-building tool is currently far from exploited. As such, by providing the output of PH into, e.g., machine learning algorithms together with information of some property of interest, correlations may be established based on the non-intuitive PH features. This has been used to couple the pore-geometry of nanoporous materials with their adsorption characteristics in crystals [81, 82]. Similarly, a number of glass properties may be suitable for such coupling with geometrical features extracted from PH, especially those associated with MRO structure. For more, the first study of such correlation between structure obtained from PH and thermal conductivity in amorphous silicon has very recently been published [83].

Chapter 3

Thermal Conductivity in Glasses

While many properties of the thermodynamical stable crystal and its isochemical glass are nearly identical, some properties show significant changes upon vitrification. One such property is that of thermal conductivity (κ). This is true even though the κ of glasses has great importance for, e.g., its influence on the performance of insulation materials, passive layers in microelectronics [7], and thermoelectric materials [84]. In addition, the thermal conductivity of the associated melt is also of great importance for optimizing melt processing and modelling [85].

3.1 Heat transfer in glasses

3.1.1 Fundamental models

The difference of thermal conductivity between crystal and glass was initially observed already in 1911 for silica by Eucken [86]. At this point, there was no physical explanation for this difference. A few decades later, significant theoretical progress was made for the understanding of κ in the crystalline state through the development of the so-called *phonon gas model* (PGM), as pioneered by Peierls [87]. Here, lattice vibrations are roughly treated as gas particles travelling in the material. By defining a velocity (v) of the phonons and length between scattering events (i.e., the *mean free path*, λ) it was possible to quantify κ as,

$$\kappa = \frac{1}{3} C_{\mathrm{V}} v \lambda = \frac{1}{3} C_{\mathrm{V}} v^2 \tau, \tag{3.1}$$

where C_{V} is the volumetric heat capacity and τ is the relaxation time (time between scattering events). Later, the same equation saw development to not

only feature single quantities, but rather be a sum over the vibrational density of states (VDOS) [88], i.e.:

$$\kappa = \frac{1}{3}\sum_i \int \frac{\mathrm{d}E_i(q,T)}{\mathrm{d}T} v_i^2(q)\tau_i(q)\mathrm{d}q, \tag{3.2}$$

where the sum is taken over all i modes. Even though Eq. 3.1 was initially developed for crystals, Kittel later reasoned how both C_V and v were rather similar for crystals and isochemical glasses [89]. As such, Kittel suggested that the main difference between crystals and glasses is the magnitude of λ and that λ of glasses eventually approach interatomic distances with increasing temperature. This idea is depicted in Figure 3.1a for SiO_2 crystal and glass.

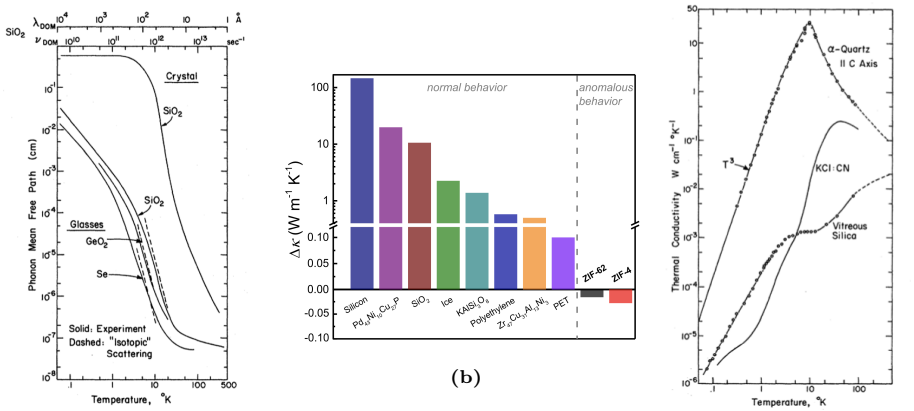

(a) (b) (c)

Fig. 3.1: (a) Phonon mean free path for a number of glassy systems as well as crystalline SiO_2 showing how crystalline mean free paths are generally orders of magnitude greater than their amorphous counterparts. (b) Comparison of the difference of the thermal conductivity in the isochemical crystalline and amorphous systems, where $\Delta\kappa = \kappa_\mathrm{crystal} - \kappa_\mathrm{glass}$. Data are obtained from Refs. [15, 90–96]. (c) Thermal conductivity of crystalline and amorphous SiO_2 at varying temperature showing a clear peak for crystalline SiO_2 (α-quartz) and the distinct plateau-behavior of the glass. Figures (a) and (c) are reprinted from Zeller and Pohl, *Phys. Rev. B*, **4**, 2029 (1971) [97]. Copyright 1971 American Physical Society. Figure (b) is reprinted from Sørensen *et al.*, *ACS Appl. Mat. Int.*, **12**, 18893 (2020) [15]. Copyright 2020 American Chemical Society.

In comparison, crystals generally feature mean free paths up to orders of magnitude greater than its isochemical glass, yet still show a qualitatively similar relation between temperature and λ as shown in Figure 3.1a. A more comprehensive comparison between the difference in thermal conductivity of glasses and their parent crystal for a diverse range of systems is found in Figure 3.1b (where $\Delta\kappa = \kappa_\mathrm{crystal} - \kappa_\mathrm{glass}$). Notably, as found in our previous work of Ref. [15] some members of the recently discovered metal-organic framework (MOF) glass family has a negative $\Delta\kappa$, i.e., the glass has a higher thermal

conductivity than its isochemical crystal. We have ascribed this strange phenomenon to be caused by the collapse of internal pores in the MOF upon vitrification (and the following increase of density) as well as the inherent large degree of disorder in the parent crystal [15].

In addition to the sole difference of κ between crystals and glasses, Zeller and Pohl [97] showed how a number of glasses feature a plateau in their thermal conductivity, typically in the range of 1 to 100 K, depending on the glass type. This case is shown in Figure 3.1c for glassy SiO_2 where the κ of the corresponding crystal is also presented, showing a sharp increase of κ followed by a sharp decrease and hence a maximum in κ at a temperature around 10 K. The found plateau has later been confirmed to be a general feature of amorphous materials and even crystals with a large degree of disorder [98] and hence required a general explanation.

3.1.2 Quantitative descriptions of thermal conductivity

This explanation was both phenomenologically and fundamentally developed in the coming 20 years through e.g., the perception of how phonon states could be localized [99] and, based on pioneering work of Einstein [100], how a minimum thermal conductivity could be envisioned [101]. The idea of a minimum thermal conductivity was simultaneously developed further into the theory of *diffusons* by Allen and Feldman [102–104]. They imagined three regimes of heat transfer, namely: i) Propagons, i.e., modes with well-defined wave-behavior, long λ, and hence significant contributions to κ. These modes are favored in well-ordered and stiff materials and are usually especially dominant for low frequency modes, even in amorphous materials [105]; ii) Diffusons, i.e., modes without a well-defined wave-character, however still with excitation of a large number of atoms in the structure. These *diffusive* modes feature lower, but nonzero, contributions to κ. Usually these modes have intermediate range eigenfrequencies; and iii) Locons, i.e., modes where only few or a single atom move. As such, these modes will transfer little or no heat and thus make negligible or no contributions to κ. These modes are typically located in the high frequency range of the VDOS. A sketch of the distribution of propagons, diffusons, and locons in the VDOS for a simulated model of amorphous Si is presented in Figure 3.2a.

In fact, these considerations were not particularly new and Klemens [88] for example gave a two-mode model (one type of vibrations based on the relative motion of neighboring atoms and another based on the movement of the structure as a whole) for glassy silica already in 1951 with a qualitative explanation of the plateau in κ with a, as Klemens state, *quite satisfactory* agreement [88]. His fit to the experimental κ of glassy SiO_2 is presented in Figure 3.2b. As such, the real contributions of Allen and Feldman were their contributions to a fundamental model quantifying the diffuson contribution to thermal conductivity in amorphous solids [102]. Until this development, modelling of thermal conductivity had, at best, been qualitative. However, Allen and Feldman sug-

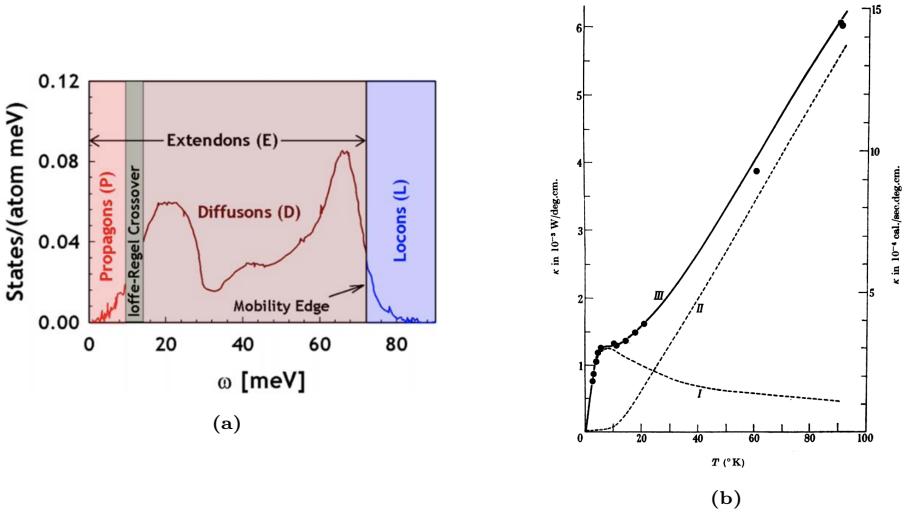

Fig. 3.2: (a) Vibrational density of states for simulated amorphous silicon with depictions of which parts of the spectral ranges belong to propagons, diffusons, and locons, respectively. (b) Plot of Klemens' two-mode model fitted to the thermal conductivity of glassy silica. Figure (a) is reprinted from Kommandur and Yee, *J. Pol. Sci., P. B*, **55**, 1160 (2017) [106]. Copyright 2017 John Wiley and Sons. Figure (b) is reprinted from Klemens, *Proc. Roy. Soc. London*, **208**, 108 (1951) [88]. Copyright 1951 The Royal Society Publishing.

gested a new description of thermal conductivity, yet in relation to Eqs. 3.1 and 3.2, the phonon mean free path and phonon group velocity would be undefined due to the lack of translational order. Instead, they would define a mode diffusivity (D_i) such that,

$$\kappa = \frac{1}{V}\sum_i C_i D_i, \tag{3.3}$$

where V is the volume of the cell studied in a molecular simulation. Now, the diffusivity is defined by [103],

$$D_i = \frac{\pi V^2}{3\hbar^2\omega_i^2}\sum_{i\neq j}|S_{ij}|^2\delta(\omega_i-\omega_j), \tag{3.4}$$

where ω_i is the frequency of the ith mode and S_{ij} is the heat current operator. Eventually, S_{ij} is based on lattice dynamics in the harmonic approximation and thus relies on the second order force constants. This is of great interest as finite thermal conductivity, as based on the phonon gas model, has previously relied on assumptions on anharmonicity. To test this new model, Allen and Feldman specifically employed atomistic models of amorphous Si to show great agreement with experiments [102, 103]. However, while the model itself has indeed been a leap in the fundamental understanding of diffusion mediated heat transfer in disordered solids, it heavily relies on access to per-atom

information. This requires a reliable interatomic potential as well as a realistic atomistic model of the studied material, greatly limiting the number of glasses which are possible to study. For this reason, Agne *et al.* [101, 107] derived a simpler model for estimating the diffuson contribution to κ, defining $\kappa_{\text{diff}}(T)$ as,

$$\kappa_{\text{diff}}(T) \approx \frac{n^{-\frac{2}{3}} k_{\text{B}}}{2\pi^3 {v_{\text{s}}}^3} \left(\frac{k_{\text{B}}T}{\hbar}\right)^4 \int_0^{0.95\theta/T} \frac{x^5 e^x}{(e^x-1)^2} \mathrm{d}x, \tag{3.5}$$

where T is temperature, k_{B} is the Boltzmann constant, n is the atomic number density, $\theta_{\text{D}} = v_s(\hbar/k_{\text{B}})(6\pi^2 n)^{1/3}$ is the Debye temperature, $\hbar$ is the reduced Planck constant, $x = \hbar\omega(k_{\text{B}}T)^{-1}$, and $v_{\text{s}} = (2v_{\text{T}} + v_{\text{L}})/3$ is the average speed of sound while v_{T} and v_{L} are transverse and longitudinal speeds of sound, respectively. Eventually, this means that only the transverse and longitudinal sound speeds, as well as the atomic number density (which is a function of composition and density) needs to be known to provide an estimate of κ_{diff}. As these four parameters are generally straightforward to determine for the majority of bulk materials (including oxide glasses), this model allows estimation of κ_{diff} for even notoriously complex systems without an atomistic model. While this naturally comes at a cost of accuracy, the applicability of the model makes it highly appealing. As such, the model will in the present thesis be used to estimate κ_{diff} for a number of oxide glasses and through a simple relation give an estimate of the propagon contribution to κ, i.e. κ_{prop}, through,

$$\kappa = \kappa_{\text{diff}} + \kappa_{\text{prop}} \Longleftrightarrow \kappa_{\text{prop}} = \kappa - \kappa_{\text{diff}}. \tag{3.6}$$

While Eq. 3.6 may only provide an estimate of κ_{diff} and κ_{prop}, it will likely be able to capture trends with changing composition and structure. At this point, both models of fully diffusive (Eq. 3.3) and fully propagative (Eq. 3.1) heat transfer have been introduced, however, for actual materials, there will be a modal distribution between these extremes despite how these may in some cases be safely neglected. Very recently, this problem was resolved independently by two groups [108, 109]. Specifically, they developed a unified theory (similar in form to Eq. 3.3) which collapse into the Allen-Feldman derivation in the harmonic case, and the PGM as derived from Boltzmann's transport equation in the anharmonic case. However, notably, their theory also allows for studying intermediate cases which see various modal contributions to κ. This method has in the present thesis been employed in Paper V for estimating κ of a series of simulated calcium aluminosilicate glasses under pressure showing good agreement with experimental data. While a detailed description of Paper V will be given in Section 4.3, Figure 3.3a presents the VDOS of a simulated 30CaO-10Al_2O_3-60SiO_2 glass (using the Matsui potential [110]) compared to experimental neutron scattering data from Ref. [111] showing a very good agreement except for a slight offset for the high frequency band around $\sim$ 30 THz.

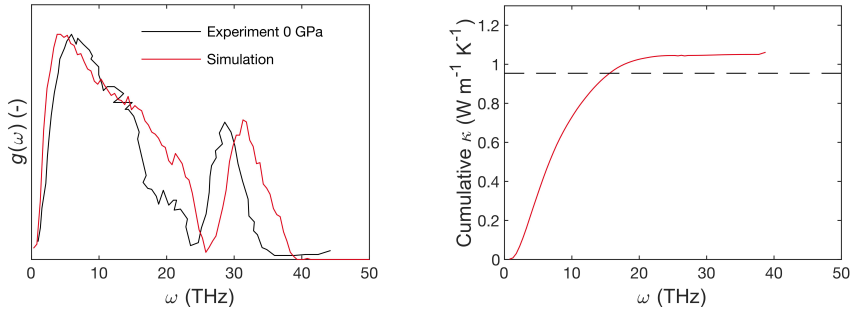

(a) (b)

Fig. 3.3: (a) Vibrational density of states ($g(\omega)$) for a simulated 30CaO-10Al_2O_3-60SiO_2 glass at 0 GPa of pressure (red) and a 43CaO-14Al_2O_3-43SiO_2 glass from Ref. [111] (black). (b) Cumulative thermal conductivity (κ) of the same simulated glass as in (a) together with the experimentally obtained total κ shown as a dashed black line. Figures (a) and (b) are plotted based on data from Paper V.

For more, the cumulative κ at 300 K for the same glass (based on the discussed unified method of heat conduction [108, 109]) is presented in Figure 3.3b where the total experimentally measured κ of the same glass is shown as a dashed black line. While a difference in the range of ∼0.1 W m^{-1} K^{-1} between simulated and experimental glass is observed, this is remarkably superior to standard methods for estimating κ (briefly discussed in Section 3.2.2) which commonly overestimates κ by a factor of two or more [12, 112]. As such the replication of κ in the 30CaO-10Al_2O_3-60SiO_2 glass system using the Matsui potential [110] is of great significance.

3.2 Measuring thermal conductivity

All of the above theories are nothing but theories and thus need to be supported by relevant measurements of κ in actual glass systems as this is a cornerstone of science. In this thesis, the most common experimental and computationally used methods for determining κ will be introduced.

3.2.1 Experimentally

Thermal conductivity is fundamentally an engineering parameter derivable from heat transfer considerations. Formally, in the isotropic case, it takes the form of a variable in Fourier's law, as [113],

$$\mathbf{q} = -\kappa \nabla T, \tag{3.7}$$

where $\mathbf{q}$ is the heat flux and ∇T is the temperature gradient. This equation directly allows to experimentally determine κ, but it commonly requires large

samples and long equilibration times to reach a steady state heat flux. However, with some derivation Eq. 3.7 allows the definition of the simple thermal diffusivity (α) metric such that:

$$\kappa = C_{\mathrm{p}}\rho\alpha. \tag{3.8}$$

While C_{p} and density (ρ) are standard variables, thermal diffusivity is a parameter which describes how quickly temperature is moved in a material. As such, determining α is the main problem for determining κ through Eq. 3.8. This may be done in several ways from which we will here mention only the *laser flash analysis* as this was the method employed in Papers III and IV to determine κ. The laser flash analysis (LFA) method is a highly versatile technique optimized to measure thermal diffusivity in a wide range of temperatures, most commonly for bulk materials [114, 115]. Practically, a finite thickness coplanar high absorbing (typically ensured by graphite or gold coating) sample is shot with a high energy laser. This instantaneously heats the sample on one side. Then, an infrared detector tracks the temperature of the sample on the opposite site of the laser. This temperature vs. time response may then be fitted to a suitable model from which α can be derived, and by combining with relevant measurements of C_{p} and ρ, κ may be obtained.

Many other techniques exist for measuring thermal conductivity, yet similarly to the LFA method, these methods often rely on measuring the time response of a temperature change, from which the data may be fitted to a model and the relevant parameters extracted (κ and/or α) [116, 117].

3.2.2 Computationally

In contrast to experimental techniques, computer simulations also allow for the determination of a range of fundamental parameters. While Section 3.1.2 has described the results of lattice dynamics, which are also of great importance in the community, MD simulations also allow for the simulation of dynamics and open new ways of determining κ. The two most common methods will here be introduced. First, Müller-Plathe developed a method [118] for determining κ based on Eq. 3.7. Here, a simulation cell is divided into a number of slabs in a given direction. Now, the energy of the most energetic atom in the boundary slab is swapped for the energy of the least energetic atom in the middle slab. This effectively increases the temperature in the middle slab of the simulation cell and consequently reduces the temperature of the boundary slabs. This case mimics that of the one-dimensional problem of the simplest solution of Fourier's law and indeed, Müller-Plathe, used an ingenious rewrite of Eq. 3.7 with the input of the summed heat transfer and the obtained temperature gradient to obtain an estimate of κ. A schematic of an obtained temperature gradient is presented in Figure 3.4a.

While this method is very useful it has been shown to be very dependent on the size of the simulation cell (L). Thus, to get reliable estimations of κ, the obtained values of κ at different box lengths are plotted as L^{-1} against κ^{-1} to

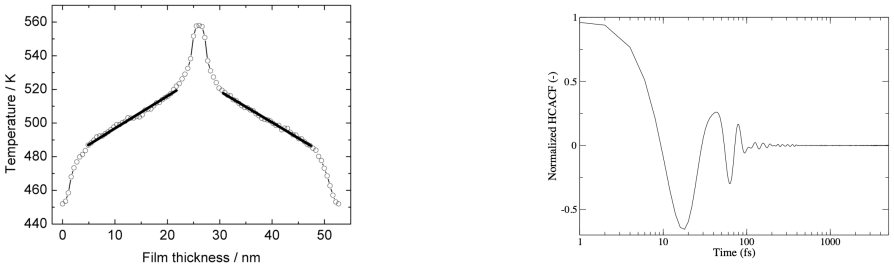

(a) (b)

Fig. 3.4: (a) Depiction of how the non-equilibrium method of Müller-Plathe will produce a temperature gradient in the simulation box when swapping low-energy for high-energy atoms, allowing for a simple deduction of thermal conductivity based on Fourier's law. (b) Principle of the equilibrium method of Green and Kubo where one obtains the heat current autocorrelation function (HCACF), here from a $35Li_2O$-$65B_2O_3$ glass. The continuous integration of the HCACF provides running κ which will typically converge within some picoseconds. Figure (a) is reprinted from Ju *et al.*, *J. Appl. Phys.*, **110**, 054318 (2011) [119]. Copyright 2011 AIP Publishing. Figure (b) is reprinted from Sørensen *et al.*, *Phys. Rev. Mat.*, **3**, 075601 (2019) [12]. Copyright 2019 American Physical Society.

then find κ_{bulk} as the $L \to \infty$ limit. However, the cumbersome procedure has been questioned to be non-linear in the $L \to \infty$ limit and thus not generally reliable [120]. For this reason, other methods are commonly used.

Contrarily to the non-equilibrium Müller-Plathe method, an alternative equilibrium method is commonly used throughout the literature (including our previous work of Ref. [12]). As derived by Green and Kubo [121–123], the thermal conductivity at a finite temperature is given as,

$$\kappa(T) = \frac{V}{3k_{\text{B}}T^2} \int_0^\infty \langle \mathbf{J}(0) \cdot \mathbf{J}(t) \rangle \mathrm{d}t, \tag{3.9}$$

where V is the the simulation box volume, $\mathbf{J}$ is the vector of the heat current, and $\langle \mathbf{J}(0) \cdot \mathbf{J}(t) \rangle$ is the so-called *heat current autocorrelation function* (HCACF). The method is commonly coined as the *Green-Kubo method*. The calculation of $\mathbf{J}$ relies on knowing interatomic forces and a suitable definition of $\mathbf{J}$. A common choice of $\mathbf{J}$ is that of Ref. [124]. While Eq. 3.9 formally requires the integration from zero to ∞ time, practically the integration is performed until convergence is reached, i.e., when $\langle \mathbf{J}(0) \cdot \mathbf{J}(t) \rangle \to 0$. An example of the normalized HCACF of a glassy $35Li_2O$-$65B_2O_3$ system studied in a previous work of ours [12] is presented in Figure 3.4b. From the HCACF, the running κ is given from integration. However, as well as for the non-equilibrium method, a number of problems exist for the Green-Kubo method. For example, for low-κ materials (like glasses), the uncertainty of the estimation of κ will often be high compared to the absolute value of κ. This forces one to do many repetitions with changing initial velocity profiles and structures to obtain reliable estimations. For more, both methods rely on a meaningful interatomic potential. This often serves as the shortcoming for making reliable

predictions of κ due to how phonon-properties are often overlooked in the literature and due to how classical potentials may greatly reproduce structure and mechanics, but utterly fail to properly reproduce the thermal properties, especially that of the vibrational density of states. For oxide glasses the most prominent potential which nicely mimics the vibrational density of states is that of Matsui, developed for calcium aluminosilicates [110, 125] while some success has been obtained for replicating the VDOS of glassy SiO_2 using other potentials [126]. The development of potentials useful for replicating phonon dynamics is, however, of rising interest [127].

3.2.3 Results of thermal conductivity in oxides

While the previous sections have provided the general framework for studying thermal conductivity in both crystalline and amorphous materials (and materials in the crossing between these limits), quite some work has been specifically dedicated to studying oxide systems beyond those studying the fundamental physics of their low-temperature anomalies. As an example, Figure 3.5 presents κ values of 244 SiO_2-containing glasses around room temperature, plotted as a function of the combined SiO_2 and B_2O_3 content.

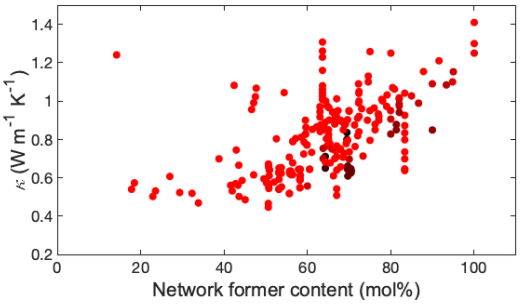

Fig. 3.5: Plot of the total thermal conductivity (κ) for 244 silicate-containing glasses as a function of the summed SiO_2 and B_2O_3 content. The color of the points represent the relative amount of SiO_2 where fully red indicates that SiO_2 is the only network-forming ion while black represents no SiO_2. Values are obtained from Refs. [2, 91, 128–142].

Although there seems to be a trend with increasing κ when increasing the network former content (Figure 3.5), the deviation is seen to be of up to a factor of three. This showcases how more rigorous testing and model building is needed to meaningfully model κ in oxide glass systems.

Multiple linear regression

An idea which a number of authors have pursued is the idea of empirically modelling the thermal conductivity of oxide glasses based on composition. Specifically, the main model is based on multiple linear regression [85, 135, 137], i.e.,

$$\kappa = \sum_i c_i \kappa_i, \tag{3.10}$$

where c_i and κ_i are the concentration and empirically fitted parameter for oxide i, respectively. While this is an intriguingly simple (and in some cases even precise [85]) way of modelling the thermal conductivity, it is in many cases a vast simplification which will provide unprecise estimations beyond the concentration ranges from which the empirical fitting parameters were obtained. As such, the model is rather applicable as an engineering tool than for fundamental understanding of the heat transfer.

The phonon gas model and diffuson contribution to κ

As initially depicted by Kittel [89] and sketched in Section 3.1.1, the phonon gas model provides a quantitative way of estimating the mean free path (λ). While λ is not a meaningful parameter for a number of modes in glassy and amorphous systems [143], it still provides a quantitative measure for comparing glass families in terms of heat transfer properties. This was, e.g., done for a number of alkali borate, alkaline earth borate, and alkali silicate glasses in our previous work of Ref. [13]. Here, it was found how λ was consequently longer in silicates ($\lambda \sim 4.35$ Å) compared to borate glasses ($\lambda \sim 3.60$ Å) with little difference when changing the modifier oxide, suggesting some differences in the fundamental heat transfer mechanisms between these two systems. Now, by applying Eq. 3.5, it was possible to access how the total thermal conductivity compared to the contribution from diffusons for these archetypical silicate and borate glasses. These results are presented in Figure 3.6 as a function of the sound speed of each glass.

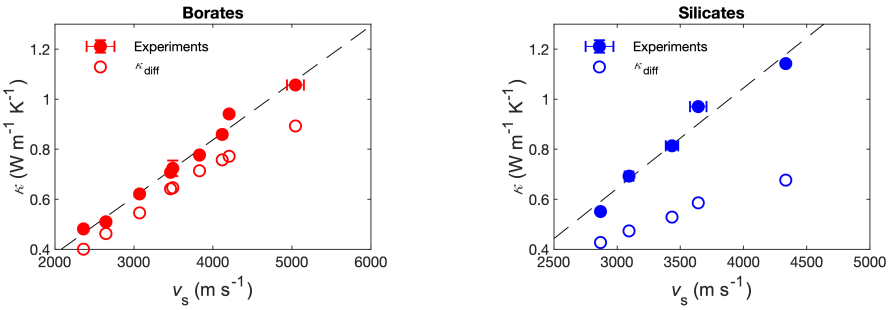

Fig. 3.6: Plot of the total thermal conductivity (κ) as well as the diffuson contribution to thermal conductivity (κ_{diff}) for (a) eight alkali and earth alkali modified borate glass as well as (b) five alkali silicate glasses as a function of their average sound speed (v_s). Figure is reprinted from Sørensen *et al.*, *Appl. Phys. Lett.*, **117**, 031901 (2020) [13]. Copyright 2020 AIP Publishing

From Figure 3.6, it is clear how the difference between κ and κ_{diff} is larger for silicates compared to borates thus following the same tendency as that of λ. The results of Figure 3.6 are intriguing for two reasons. First, κ is seen to correlate rather nicely with the average sound speed - a parameter which is closely coupled with structure and rigidity of the underlying network. Second, as established in Chapter 2, the structural differences in these two glass families are significant. This result of diffusive and total thermal conductivity in archetypical borates and silicates thus suggest that network structure and rigidity do indeed provide contributions to κ in oxide glasses. This is the main outcome of the current thesis and will be explored in more detail in the next, and final, chapter.

Chapter 4

Correlating glass structure and thermal conductivity

Crystalline structure and κ are generally known to be closely coupled, especially when comparing highly disordered and ordered crystalline materials, for which the latter will see significantly higher κ. This effect is mainly apparent in high-rigidity materials, e.g., diamond [144, 145] where even exchanging of isotopes can greatly impact λ and hence also κ. However, in the amorphous case, disorder is the inherent fingerprint of the structure. In such case, the picture is much more complex.

4.1 Structural anomalies and thermal conductivity

4.1.1 Binary oxide systems

To initiate a coupling between atomic structure and κ, meaningful correlations need to be established. An approach for understanding such correlation is thus to *change* the structure and then record the following response of κ. This may be done using composition or external parameters, e.g., pressure. However, such change will often be linear and, as such, difficult to correlate unambiguously. For this reason, it is ideal to initiate the search for a structural correlation to κ in systems which show anomalous structure with, e.g., changing composition. As discussed in Section 2, this is the case for glasses containing borate and germanate and therefore these glasses are ideal for studying the sought fundamental correlations.

Initially, in our previous work of Ref. [12], a series of $x\mathrm{Li_2O}(100-x)\mathrm{B_2O_3}$ (where x ranged from 0 to 48) glasses were studied at room temperature using both experiments and simulations. This compositional range was chosen to fully encapsulate the transformation of three to four-coordinated boron and

then the following reversion of boron CN with further modifier addition. The relative amount of four-coordinated boron (N_4) of the studied glasses are presented in Figure 4.1a while the thermal conductivity of these glasses is presented in Figure 4.1b.

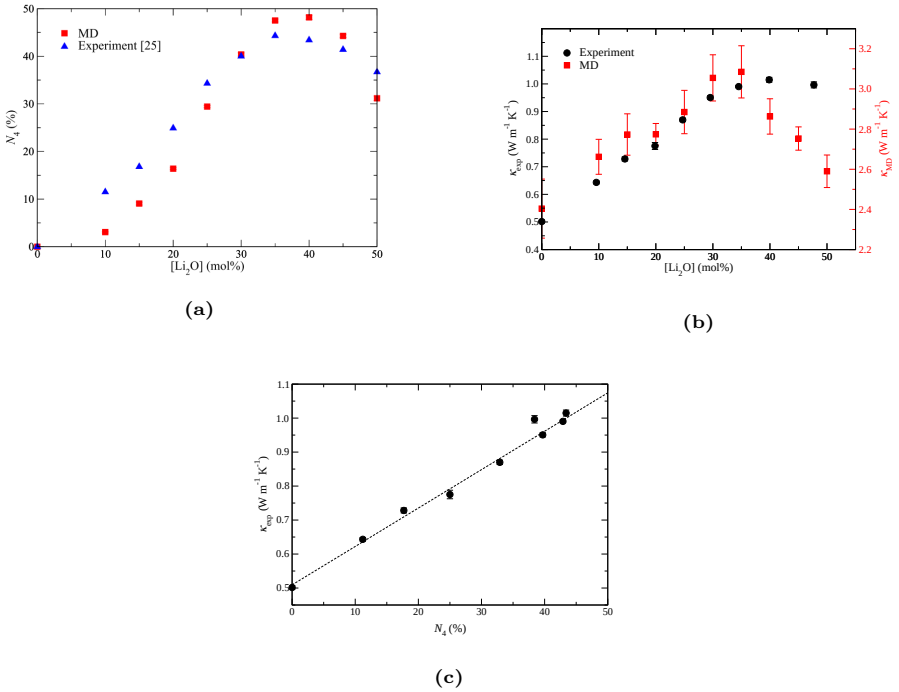

Fig. 4.1: (a) Relative fraction of four-coordinated boron (N_4) as a function of the Li_2O content in the $x$$Li_2O$-(100-$x$)$B_2O_3$ glass series. (b) Thermal conductivity (κ) of experimental and simulated glasses in lithium borate series as well as (c) the correlation between the number of four-coordinated boron (N_4) and experimental κ. Figures (a), (b), and (c) are reprinted from Sørensen *et al.*, *Phys. Rev. Mat.*, **3**, 075601 (2019) [12]. Copyright 2019 American Physical Society

Here, for both experiments and simulations, an increasing κ with increasing Li_2O-content is found up until ∼35-40 mol% before a decrease is found. Interestingly, this is very much on par with the change of a number of other parameters and quite similar to the maximum in the amount of four-coordinated boron in this glass system (Figure 4.1a) [146, 147]. In fact, when plotting κ as a function of the fraction of four-coordinated boron (N_4), a strong correlation is found (see Figure 4.1c), except for a slight deviation at higher Li_2O concentrations. This is interesting given how a series of sodium borate glasses were previously measured where no direct correlation was found, likely due to exploring a too narrow composition range [148]. While there exist no direct comparison for the glassy state, Kim and Morita [149] studied a potassium

borate melt at 1000 °C to find a qualitative correlation like that shown in Figure 4.1c.

While these are interesting cases for the alkali borate system, other anomalous systems are also of great interest. One such is that of lithium germanate glasses (i.e., $x\mathrm{Li_2O}$-$(100-x\mathrm{GeO_2})$ with $x = \{5, 10, 15, 20, 25, 30\}$), as studied in Paper IV of the present thesis. This system was chosen due to its anomaly, its ease of preparation, and due to the possibility to compare with the previously studied lithium borate glass series. Generally, it is known that alkali germanate glasses will show a sharp increase in Ge coordination until around 18 mol% of modifier, before the CN of Ge decreases again towards a Ge CN of 4. This correlation of alkali oxide content and average Ge CN is shown in Figure 4.2a as obtained from Ref. [27]. However, upon increase of the $\mathrm{Li_2O}$ concentration, κ of the lithium germanate system at room temperature first increases, then decreases, and then shows a further increase in κ for the $30\mathrm{Li_2O}$-$70\mathrm{GeO_2}$ glass. This effect is shown in Figure 4.2b together with the calculated κ_{diff} as calculated based on Eq. 3.5. When comparing Figures 4.2a and 4.2b it is interesting to observe that despite the initial increase of both Ge CN and κ, the high $\mathrm{Li_2O}$ content glasses does not seem to follow the same trend for the Ge CN and κ.

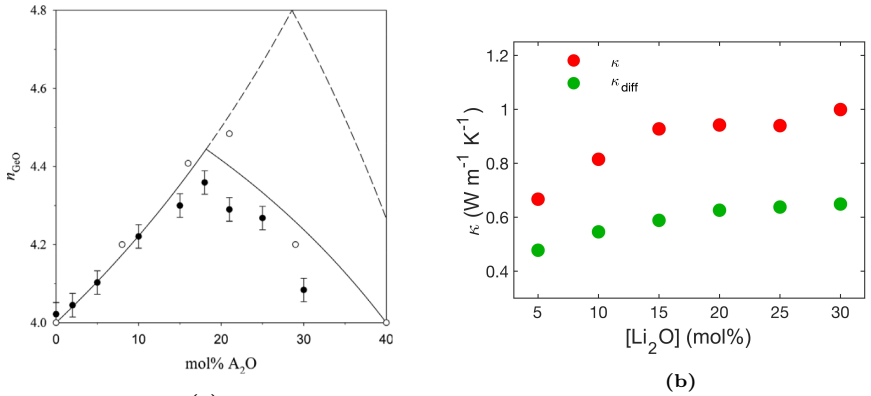

Fig. 4.2: Average Ge coordination number in sodium germanate (open circles) and cesium germanate (closed circles) glasses as obtained from neutron diffraction. Full and dashed lines are results of models ascribing the coordination number change of Ge to 5 or 6, respectively. (b) Total thermal conductivity (κ) and diffuson contribution to thermal conductivity (κ_{diff}) for a series of $x\mathrm{Li_2O}$-$(100\text{-}x)\mathrm{GeO_2}$ glasses. Figure (a) is reprinted from Hannon *et al.*, *J. Non-Cryst. Solids*, **353**, 1688 (2007) [27]. Copyright 2007 Elsevier. Figure (b) is reprinted from Paper IV.

When comparing the results of lithium germanates with those of lithium borates, it is thus noteworthy how high modifier content glasses will tend to deviate from a clear direct correlation to coordination. From these results it seems reasonable to suggest that their exist two contributions to thermal conductivity in the case of oxide glasses and that structure does somehow impact

the total κ, in some resemblance with previous models [88, 102]. However, the presented results provide only a qualitative measure of this effect and thus to extend the possibilities of building a more quantitative answer to this scientific peculiarity, it is of great interest to further study other systems of anomalous behavior.

Before introducing such systems, it is worth noting how κ of the studied lithium germanate series, in similarity to the results of Figure 3.6, show a very nice correlation with the average sound speed, i.e. $v_s = (v_L + 2v_T)/3$. This correlation is shown in Figure 4.3 for both the glasses studied in Paper IV as well as literature data from Refs. [12, 13, 131, 136, 150–152].

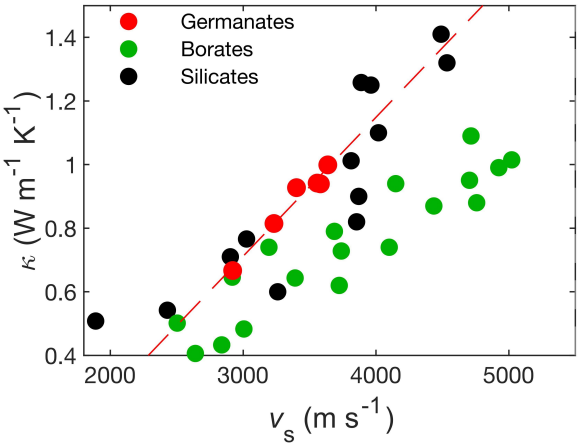

Fig. 4.3: Thermal conductivity (κ) as a function of average sound speed ($v_s = (v_L + 2v_T)$ for a number of modified germanate, borate, and silicate glasses from Paper IV and Refs. [12, 13, 131, 136, 150–152]. Figure is reprinted from Paper IV.

Despite being a relatively simple correlation, which provides no direct correlation to structure, its simplicity is compelling. From a more fundamental point of view, it is also worth noting how κ correlates linearly to sound speed in both the phonon gas model (Eq. 3.1) as well as in the high temperature limit of the estimation of κ_{diff} (Eq. 3.5 [107]), i.e.,

$$\kappa_{diff}(T \to \infty) \approx 0.76 n^{2/3} k_B v_s. \tag{4.1}$$

Although simple, these results of a correlation between v_s and κ in a number of simple glasses may aid in the design of oxide glasses of either very high or low κ. This is especially compelling given how models of predicting density and elastic moduli of oxide glasses are seeing increasing interest in the literature [153–155], and the inherently simple relationship between these parameters and sound speed in glasses [156]. However, as will be shown in the next section, the linear correlation does not necessarily extend to more complex glasses, e.g., those of Paper III.

4.1.2 Mixed network former glasses

Besides the simple binary oxide systems, anomalous structural behavior may also be seen when introducing a more complex glass composition, e.g., in mixed network former glasses. The most common mixed former glass is likely that of the combination of silicate and borate, i.e., the borosilicate system. Such system is studied in Paper III as a series of 15CaO-10Na_2O-xB_2O_3-(75-x)SiO_2 glasses with $x = \{0, 6, 12, 24, 37, 51, 63\}$. These glasses were hot compressed (up to 2 GPa) and subsequently probed for their structure and thermal conductivity at room temperature. While compositionally somewhat more complex than the previously studied binary systems of Paper IV and our previous works of Refs. [12, 13], the soda lime borosilicate series pose an industrially relevant glass series. For more, it is of great importance that this specific series has seen the development of a notably successful model of topological constraints [68]. The absolute concentration of four-coordinated boron as measured from NMR spectroscopy for all studied borosilicate glasses is presented in Figure 4.4a.

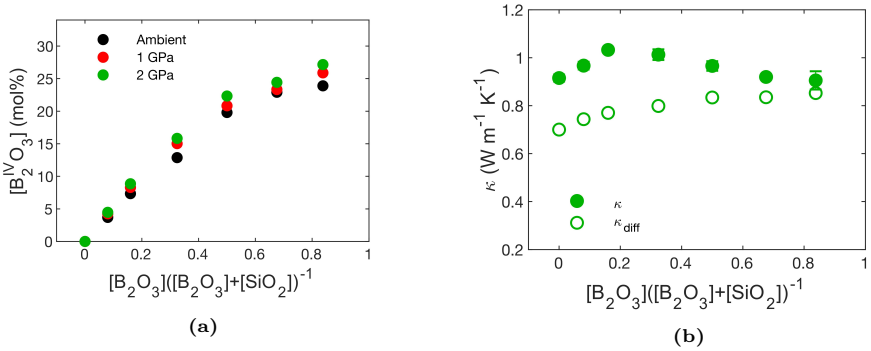

Fig. 4.4: (a) Absolute amount of four-coordinated boron in a series of pristine and hot compressed (at 1 or 2 GPa) 15CaO-10Na_2O-xB_2O_3-(75-x)SiO_2 glasses. (b) Thermal conductivity (κ) and diffuson contribution to thermal conductivity (κ_{diff}) for the soda lime borosilicate glasses hot compressed at 2 GPa of gas pressure. Figures (a) and (b) are reprinted from Paper III.

From Figure 4.4a, a generally increasing amount of four-coordinated boron with increasing borate content in the borosilicate system is found. This tendency is mimicked for other simple structural metrics, e.g., the packing density (Paper III). For more, the difference upon hot compression is seen to be slightly larger for glasses of higher B_2O_3 content.

Now, measurements of the thermal conductivity and related calculated κ_{diff} of the glasses hot compressed at 2 GPa are presented in Figure 4.4b. This plot shows how the diffuson contribution to κ, like for the lithium germanates (Figure 4.2b), shows a monotonically increasing trend, yet that there is a clear maximum in the total κ for the $x = 12$ glass. This discrepancy between κ_{diff} and κ again stresses how there seems to be a structural component to the thermal

conductivity, yet that structure does not fully explain the found trends. As shown, the same is the case for lithium borates and germanates. As such, this finding calls for a need to couple to a meaningful property or structural metric. Given the success of coupling to v_s for the compositionally simpler binary oxides (Section 4.1.1), such approach was also tested for the borosilicates of Paper III. The resulting plot of the uncompressed (ambient) and hot compressed (at 1 and 2 GPa) glasses are presented in Figure 4.5.

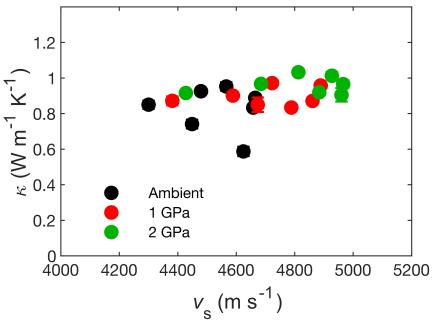

Fig. 4.5: Plot of total thermal conductivity (κ) at room temperature as function of average sound speed ($v_s = (v_L + 2v_T)/3$). Figure is reprinted from Paper III.

In Figure 4.5 it is observed how especially the uncompressed borosilicate glasses see no clear correlation between v_s and κ. This result suggests that the simple correlation between v_s and κ is exactly that - too simple. For this reason, Papers III and IV have been somewhat devoted to establishing a more comprehensive description of the contributions to thermal conductivity in oxide glasses.

4.2 Coupling thermal conductivity and structure

As shown in Figure 4.4 (reprinted from Paper III), unlike for lithium borates [12], the coordination number is not a meaningful metric to employ across a wider range of oxide glasses for correlating to κ. Now, instead of focussing on simple per-atom based structural metric - it is suggested to look at a metric encompassing the structural rigidity of the whole network. A meaningful metric to use for this is the number of *contraints* per atom, as described by topological constraint theory (see Section 2.4.2).

An initial observation which laid the foundation for seeking this coupling was done for the studied borosilicate glasses of Paper III. By comparing Figure 4.6a with the number of constraints per atom, a compelling overlap was found. This may be seen when comparing Figures 4.6a and 4.6b where a clear

maximum is seen for κ and the average number of atomic constraints at an approximately similar composition.

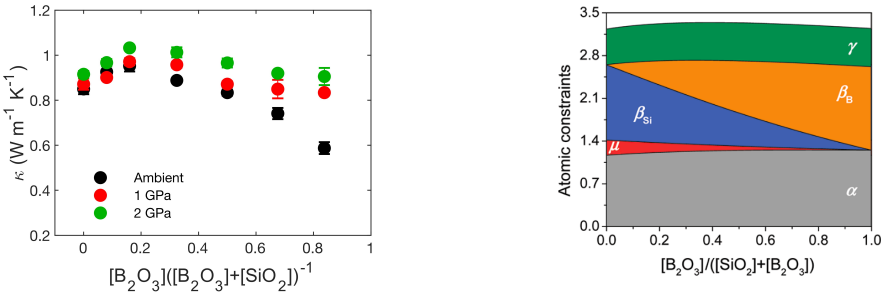

Fig. 4.6: (a) Total thermal conductivity (κ) of a series of uncompressed and hot compressed (at 1 and 2 GPa) 15CaO-10Na_2O-$x$$B_2O_3$-(75-$x$)$SiO_2$ glasses. (b) Average number of constraints per atom for the studied soda lime borosilicate glasses as well as the their individual constraint contribution (α, β, γ, and μ are different types of constraints). A clear maximum is seen for the total number of constraints in the region of $[B_2O_3]/([SiO_2]+[B_2O_3])\sim0.2$. Figure (a) is reprinted from Paper III. Figure (b) is adapted from Smedskjær *et al.*, *J. Phys. Chem. B*, **115**, 12930 (2011) [68]. Copyright 2011 American Chemical Society.

Relations between thermal conductivity and the average number of atomic constraints have previously been suggested in the literature, e.g., in some of the original works on TCT of Thorpe [63] who suggested that there would be a change in κ below the rigidity threshold (i.e., $n_c < 3$). Other works on amorphous chalcogenide, fluorocarbon [157–159], and Si-based thin film compounds have shown such correlations to be largely correct. However, many of these systems are considerably simpler (allowing, e.g., easy assessment of coordination numbers) than the multicomponent oxide systems considered in this thesis. This makes the previous results difficult to transfer directly to the systems studied in the present work.

In this thesis, instead of directly correlating to n_c, an approach originally developed for predicting Vicker's hardness [160] will be taken. That is, instead of using the average number of atomic constraints (n_c) the *volumetric constraint density* (n_c') will be employed as it has empirically been found to provide better correlations with κ_{prop}. Fundamentally, this would also be meaningful when considering the great impact of atomic number density (and density in general) on κ - something which is not directly considered when only employing n_c. The n_c' metric is defined as,

$$n_c' = \frac{n_c \rho N_A}{M_{ave}}, \tag{4.2}$$

where n_c is the average number of atomic constraints, N_A is Avogadro's number, and M_{ave} is average molar mass based on the oxides, i.e.,

$$M_{\text{ave}} = \sum_{i}^{n} x_i M_i, \tag{4.3}$$

where x_i is the molar fraction of oxide i and M_i is its molar mass. An example of the difference in n_c and n_c' for the lithium germanate system studied in Paper IV is presented in Figure 4.7 showing a remarkable difference in the maximum of n_c as compared to n_c'.

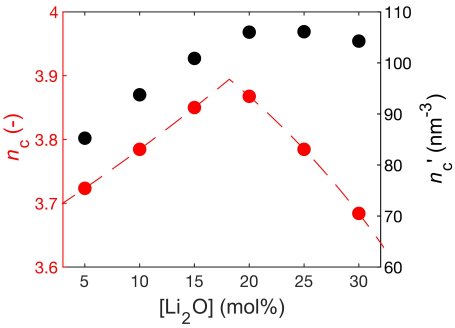

Fig. 4.7: Average number of atomic constraints (n_c, red points, left axis) and volumetric constraint density (n_c', black points, right axis) for a series of xLi$_2$O-(100-x)GeO$_2$ glasses. Figure is reprinted from Paper IV.

Now, while a direct relation with κ would be highly intriguing, such correlation will only in some cases provide a reasonable fit (see Figures 8b and S8 in Paper III). Rather, in this thesis, the idea of two fundamental contributions to κ will be taken. As suggested in Eq. 3.6, the contribution of diffusive (κ_{diff}) and propagative (κ_{diff}) modes will be considered. First, κ_{diff} may be described through Eq. 3.5 with only four parameters, namely, temperature, composition, density, and average sound speed. One may argue that, under a constant thermal and pressure history, the latter three parameters may be described only as a function of the composition. As stated in Eq. 4.1, $\kappa_{\text{diff}}(T \to \infty) \propto v_s$ and as many glasses at room temperature will be close to or above their Debye temperature, Equation 4.1 serves as a useful expression for the approximate calculation of qualitative changes of κ_{diff}. For more, Eq. 4.1 may serve as an engineering parameter, i.e., to tweak total κ. For example, for obtaining high values of κ_{diff} one should design glasses of high n and v_s. This usually means employing low molecular weight high field strength oxides which will create dense rigid networks, maximizing n and v_s, and hence also maximizing κ_{diff}. The opposite should be the case for decreasing κ_{diff}. Despite the simplicity of Eq. 4.1 it is noted to the reader how the temperature-dependent equation for estimation κ_{diff} (i.e., Eq. 3.5) was used for calculating κ_{diff} in Papers III and IV, despite being slightly more cumbersome. Second, based on the shown differences between total κ and κ_{diff} in both Paper III and IV it will be assumed that there exists an additional contribution to κ. This contribution should be

κ_{prop} and, as will be shown, have an intriguing correlation with n_c'. The general idea of separating κ_{diff} and κ_{prop} is sketched in Figure 4.8.

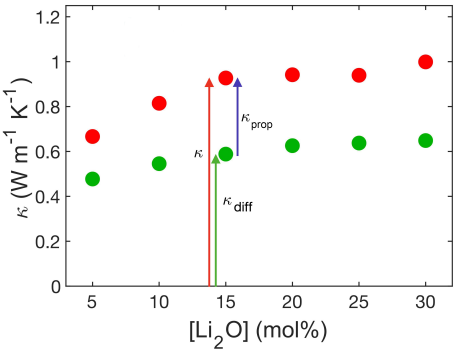

Fig. 4.8: Depiction of the contribution from diffusive (κ_{diff}) and propagative (κ_{prop}) modes to total thermal conductivity (κ). Figure is adapted from Paper IV.

While a quantitative description of κ_{prop} based on simple parameters is still not present, as suggested, κ_{prop} may be estimated by knowing κ_{diff} and the total κ (Figure 4.8). Performing this data reduction and plotting as a function of n_c' for the studied borosilicate glasses of both uncompressed and glasses hot compressed at 1 and 2 GPa (Paper III), an intriguing collapse of data is found as presented in Figure 4.9a.

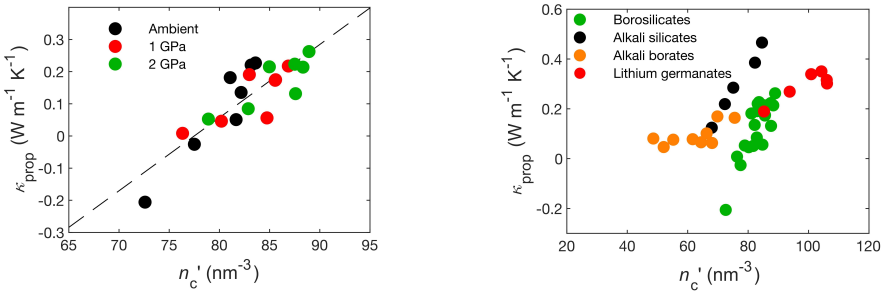

(a) **(b)**

Fig. 4.9: Contribution of propagons to thermal conductivity (κ_{prop}) for (a) pristine and hot compressed 15CaO-10Na_2O-$x$$B_2O_3$-(75-$x$)$SiO_2$ glasses together with (b) other series of alkali silicates, alkali borates, and lithium germanate glasses. All values are at room temperature. Figures (a) and (b) are reprinted from Papers III and IV, respectively.

While the approximation of κ_{diff} is obviously not precise, as seen by some κ_{prop} below 0 (i.e., $\kappa_{\text{diff}} > \kappa$), the linear tendency of Figure 4.9a is somewhat convincing. An extension of the range of glasses to other previously studied oxide glasses (from Paper III, Paper IV, as well as our previously published works

of Refs. [12, 13]), shows how the linear tendency seems to largely persist across various glass families including alkali borate, alkali silicate, lithium germanate, and borosilicate glasses as based on Papers III, IV, and Refs. [12, 13].

However, instead of collapsing onto a single curve, each glass family seems to have an independent slope in the n_c' vs. κ_{prop} plot. For now, this correlation remains unexplored and may be heavily affected by even small inconsistencies in estimating κ_{diff}. Despite this, an interesting observation may be noted. That is, how borates occupy a largely horizontal correlation with increasing n_c' in Figure 4.9b while the other glass families see a clearly nonzero slope. Considering the underlying coordination numbers, it is worth noting that the average coordination number in the borate glasses is the lowest of the studied systems [2]. This could be a possible explanation for the differences found for the slopes, but this requires more in-depth analysis of more glass families to establish such kind of correlation. For example, this does not fully comply with how the Ge CN would averagely be expected to be above 4 while the CNs of B and Si in silicate and borosilicate would be between those of borate and germanium.

4.3 Thermal conduction in glasses under pressure

The general content of Papers III and IV with the development of a model correlating n_c' and κ_{prop} was described in the previous section. However, it is worth noting how Paper III was dual-sided. That is, it studied both a change of composition as well as the effect of hot compression on the studied borosilicate glass series. In regard to the effect of hot compression treatment it is seen from Figure 4.4a how borate rich glasses tend to see a much more pronounced increase in κ upon hot compression compared to silica-rich glasses. While this is indeed explained by the increase in κ_{diff} and n_c', it is interesting how the overall structural compression is largely unexplained by both the coordination number (Figure 4.4a) and n_c' metrics. Aside from the presented correlations an association between the change of the absolute amount of four-coordinated boron per GPa of hot compression and the change of κ ($\Delta\kappa$) was sought as presented in Figure 4.10a. Here, a positive, yet weak, correlation was found, thus not providing a clear tendency for further exploration, despite how this would be rather meaningful given the previously found close correlation between N_4 and κ [12]. Measurements of simpler hot compressed boron-containing glasses would be interesting to study to better probe the correlation in Figure 4.10a.

Another common metric for studying compression is however interesting, namely that of atomic packing density (C_g). C_g fundamentally describes the amount of filled space in the glass structure based on simple assumptions on coordination numbers and ionic radii of each atomic species [161]. The C_gs of both uncompressed as well as hot compressed borosilicates are presented in Figure 4.10b showing a general increase in C_g with compression for all studied

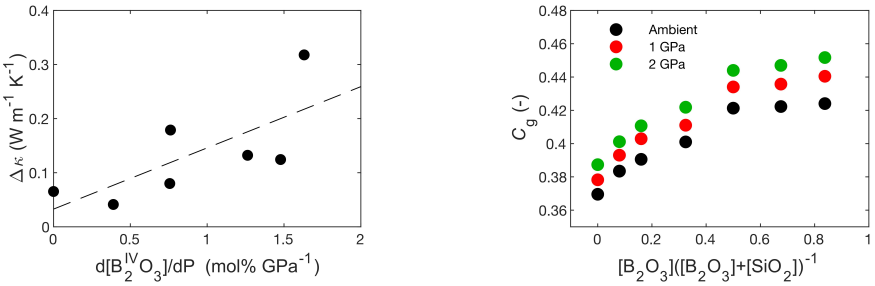

Fig. 4.10: (a) Change of thermal conductivity ($\Delta\kappa$) as function of the change of absolute four coordinated boron per GPa of hot compression from 0 to 2 GPa. (b) Atomic packing density (C_g) of the studied borosilicate glasses from Paper III as a function of their boron content. Figures (a) and (b) are reprinted from Paper III.

glasses, however, with a slightly more pronounced increase for glasses of higher borate content.

From Figure 4.10b a similar large jump of C_g for the pure silicate glass is found. The C_g jump is comparable to the borate glasses of nearly similar composition. At these pressures, no change of Si coordination would be expected and thus differences of structure upon compression would be expected to rely on medium-range order changes. As such, medium-range order structure must inherently play a role in the densification process, albeit that the identification of a structural fingerprint is beyond the extend of the current thesis.

The empirical studies presented in the previous section serves as an interesting correlation between structure and thermal conductivity in oxide glass systems. Especially when considering how detailed information on phonon properties and structure is extremely difficult to acquire experimentally for a single glass, not to mention, for a range of glasses. However, as stated, the experimental deductions come with a range of shortcomings. For this reason, some work has been devoted to understanding a single glass composition in depth through the use of MD simulations. While experiments always provide the final confirmation of predicted behavior, modelling and simulation techniques continue to strengthen their position as indispensable methods in the natural sciences for both predicting experimentally inaccessible conditions or deepening the understanding of observed phenomena. The same is true within glass science where modelling continues to see larger contribution [9]. However, while structural and mechanical studies are common [42, 162], studies of vibrational character and especially κ of oxide glass systems are inherently scarce in the current literature, not to mention the effect of κ when changing the thermal and pressure history.

4.3.1 Vibrational characteristics and structure of an archetypical oxide glass under pressure

Despite the lack of literature, this section will be devoted to such exploration of an archetypical oxide glass under pressure to showcase the possibilities of the MD technique, namely through a $30CaO\text{-}10Al_2O_3\text{-}60SiO_2$ glass. The arguments for choosing this glass composition are dual-sided. First, it resembles many of the structural features found in a range of oxide glasses of industrial and scientific relevance [6, 125, 163, 164]; Second, it is one of the few glasses for which there exist a force field capable of nicely reproducing the vibrational character of the system (e.g., the vibrational density of states). However, to not only study a single glass composition, its pressure dependency has also been studied in the interval of 0 to 100 GPa. This is of importance in, e.g., geology and for the fundamental understanding of the pressure response of such systems. For the $30CaO\text{-}10Al_2O_3\text{-}60SiO_2$ glass, the vibrational density of states (VDOS) is very well-reproduced in the unpressurized state as presented Figure 4.11a while the VDOS see significant smearing upon increasing pressure.

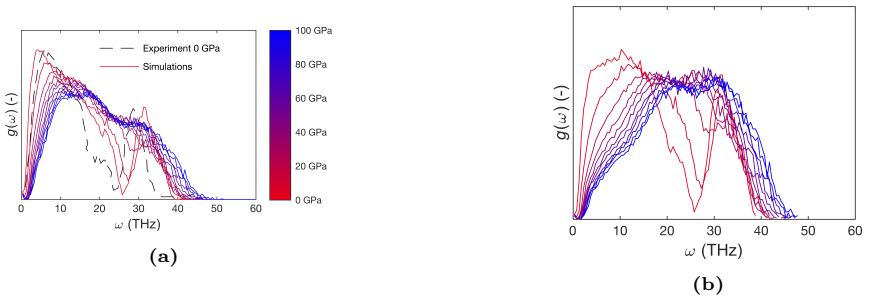

Fig. 4.11: (a) Total and (b) partial oxygen vibrational density of states for simulated compressed $30CaO\text{-}10Al_2O_3\text{-}60SiO_2$ glasses from 0 to 100 GPa as indicated by the colorbar. The dashed line in (a) is an experimental spectrum of the full VDOS of a $43CaO\text{-}14Al_2O_3\text{-}43SiO_2$ glass as obtained from neutron scattering in Ref. [111]. Figures (a) and (b) are reprinted from Paper V.

Compositionally, it may be shown how the majority of modes feature a large amount of oxygen vibrations (see the partial VDOS of oxygen in Figure 4.11b) which contribute both to the low frequency band from 0 to $\sim$ 20 THz yet also to the higher frequency band at 25 to 40 THz. This is also the case for silicon in the glasses, while calcium and aluminium mainly see contributions to the lower frequency band. Additionally, the two bands are seen to merge when increasing the pressure of the sample while quenching (Figure 4.11a).

Structurally, the overall reproduction of the real uncompressed glass is also convincing when comparing the calculated neutron structure factor (Figure 4.12a), despite for some minor differences in intensity of the FSDP.

With the increase in pressure, significant structural rearrangement is also observed. Most notably is perhaps the changes in local coordination numbers

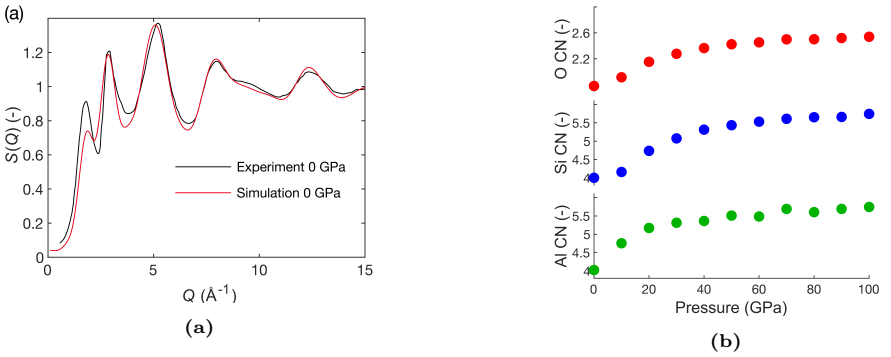

Fig. 4.12: (a) Comparison of simulated (red) and experimental (black) neutron structure factor ($S(Q)$) of a 30CaO-10Al_2O_3-60SiO_2 glass at 0 GPa. (b) Coordination numbers of Al, Si, and O in 30CaO-10Al_2O_3-60SiO_2 glasses from 0 to 100 GPa. Figures (a) and (b) are reprinted from Paper V.

of the network-forming species, i.e., silicon, aluminium, and oxygen. Their CNs are shown as function of the pressure in Figure 4.12b. Here, general increases of CNs are observed for all three atomic species, however with some differences. Specifically, while Al sees significant CN alteration already in the "low" pressure regions (<20 GPa), oxygen and silicon first see major increase of their CNs when reaching and surpassing 20 GPa of pressure. Such difference between especially aluminium and silicon is also found experimentally [165].

4.3.2 Changes of thermal characteristics

Now, the real advantage of simulations lie in the accessibility to atomic forces. Applying the recently developed unified method of estimating κ requires the use of harmonic and anharmonic force constants (to the third order). These are readily available from simulation models, although at an extreme computational expense (due to how computing the total number of third order force constants scale as $(3N)^3$ with N being the number of atoms in the simulation cell). For the present CAS system this was the argument for only studying simulations sizes of approximately 500 atoms. For the studied CAS system, the analysis of κ provide an interesting correlation with first sharply increasing κ from $\sim$1 W m^{-1} K^{-1} at 0 pressure to 1.6 W m^{-1} K^{-1} at 40 GPa. Next, κ largely levels off at $\sim$1.7 W m^{-1} K^{-1} when approaching 100 GPa of pressure. The full correlation of pressure and κ is presented in Figure 4.13a.

In addition to the total κ, the unified method of heat transfer also allows for the calculation of the cumulative κ as presented in Figure 4.13b. Here it is seen how low frequency modes provide significant contributions to κ yet that the pressure response is mainly governed by modes of higher frequencies (>15 THz).

Apart from the simulations, the 30CaO-10A_2O_3-60SiO_2 glass was also pre-

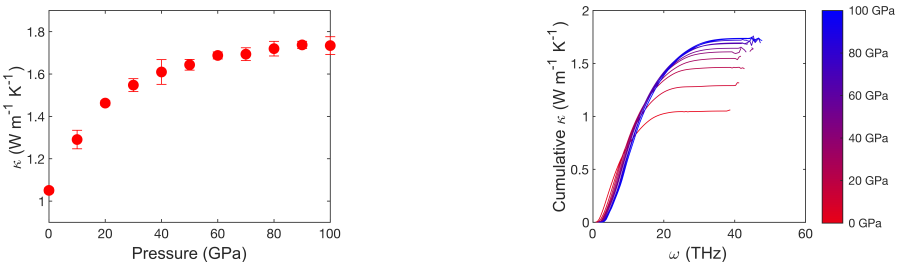

Fig. 4.13: (a) Total and (b) cumulative thermal conductivity of compressed 30CaO-10Al_2O_3-60SiO_2 glasses from 0 to 100 GPa at 300 K. Figures (a) and (b) are reprinted from Paper V.

pared experimentally through the melt-quench method and hot compressed to 1 GPa of pressure. Notably, the pristine and hot compressed glasses featured thermal conductivities of 0.954 and 0.995 W m^{-1} K^{-1}, respectively. This is in remarkable agreement with the experimental data and together with the shown VDOS agreement, this shows that the used force field parameterization (Matsui *et al.* [110]) provides a very good description of the vibrational characteristics of this glass material. A compelling observation is also how the pressure response of thermal conductivity in the low-pressure region is very similar for the simulated and experimental glasses (∼0.03 and ∼0.04 W m^{-1} K^{-1} GPa^{-1}, respectively). This strengthens the believe that the simulations are meaningful for replicating the pressure response of these glasses, at least at low pressures. As described in Section 3.2.2, the calculation of κ involves the determination of a modal diffusivity. Such estimation of diffusivity is shown in Figure 4.14a for the studied CAS glasses under pressure.

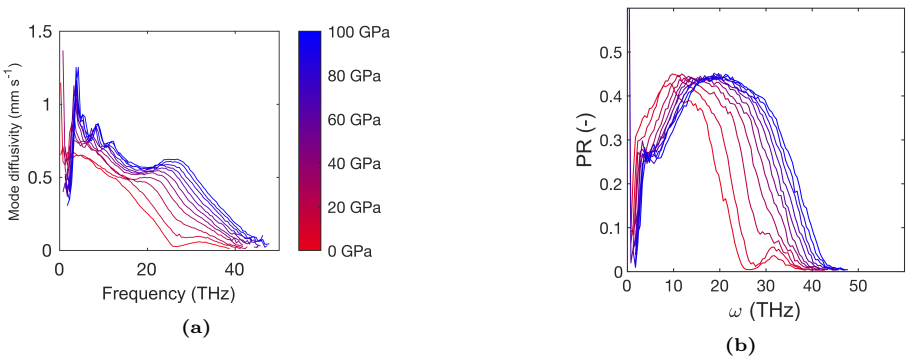

Fig. 4.14: Binned (a) mode diffusivity and (b) participation ratio (PR) for compressed 30CaO-10Al_2O_3-60SiO_2 glasses from 0 to 100 GPa. Figures (a) and (b) are reprinted from Paper V.

Here, it is shown how the diffusivity is significantly higher for low frequency modes (<15 THz), yet that increasing pressure notably increases the modal diffusivity of high frequency (>15 THz) modes. This is consistent with the cumulative κ (Figure 4.13b) which mainly see differences in the contribution to κ for higher frequency modes. However, why is this the case? To answer this, a rather simple modal characteristic will be computed, that is, the *participation ratio* (PR), defined by,

$$PR_i = (N \sum_{n}^{N} |\bar{e}_{n,i}|^4)^{-1}, \tag{4.4}$$

where PR_i is the participation ratio of mode i and $\bar{e}_{n,i}$ is the eigenvector of atom n in mode i. As eigenvectors are normalized so that [59],

$$(\mathbf{e}_i)^{\mathrm{T}} \cdot \mathbf{e}_j = \delta_{ij}, \tag{4.5}$$

it may easily be shown how the limits of PR are $1/N$ for a mode with only a single atom moving, while a mode with equally distributed movements of all atoms will feature $PR_i = 1$. The binned PR for modes is shown in Figure 4.14b. Similarly to the diffusivity and cumulative κ, the PR sees significant increases for modes in the frequency range of 15 to 40 THz. Interestingly, PR is the usual metric to distinguish localized from extended (that is, diffusive and propagative) modes, simply by defining a lower cutoff (typically a locon is taken as a mode with $PR < 0.15$). By doing this for the studied CAS system, one may plot the amount of extended modes as a function of pressure as presented in Figure 4.15a.

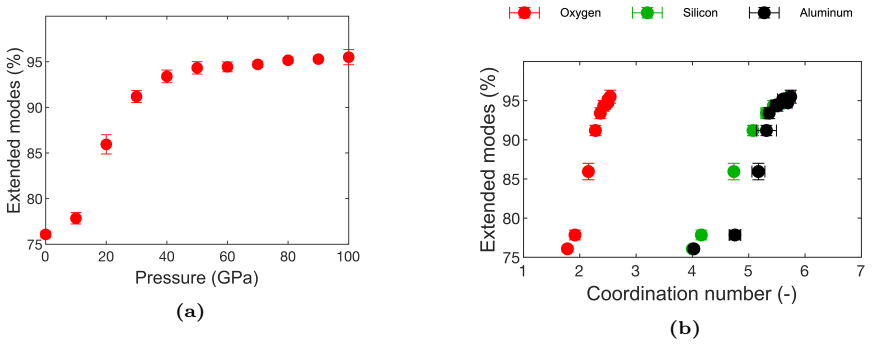

(a) (b)

Fig. 4.15: (a) Number of extended modes (i.e., non-locons) as a function of compression pressure in 30CaO-10Al_2O_3-60SiO_2 glasses from 0 to 100 GPa. (b) Correlation between coordination numbers of O, Si, and Al and the number of extended modes. Figures (a) and (b) are reprinted from Paper V.

This provides a correlation where the amount of extended modes increases from ∼75% to ∼95% when increasing the pressure from 0 to 40 GPa of pressure,

before the amount of extended modes levels off in the range of 40 to 100 GPa. Comparing this correlation with the coordination numbers of oxygen, silicon, and aluminium (Figure 4.12b), a striking similarity to the correlations of oxygen and silicon is found. The direct correlation between the relative amount of extended modes as a function of the ion coordination number for oxygen, silicon, and aluminium is plotted in Figure 4.15b. Contrarily to oxygen and silicon, aluminium is not seen to have as direct a correlation between the number of extended modes and CN. This may seem obvious, as oxygen and silicon are the main atomic species in the network, but the result is also of great interest as it provides a structural correlation between localization and coordination numbers (and thus, principally, also rigidity). While more systems need testing before being able to consider this a general rule extending beyond the current CAS system and used compression method, the provided results are encouraging in terms of establishing the fundamental correlation between modal behavior, κ, and structure.

Another interesting feature of the CAS system is how the so-called *boson peak* (BP) shows major changes when changing the pressure of the system. Fundamentally, the boson peak is an excess of vibrational modes beyond that expected by Debye theory [166]. As Debye theory predicts $g(\omega) \propto \omega^2$, the most common method for observing the boson peak is by transforming the VDOS (i.e., $g(\omega)$) by ω^{-2} as this will make the Debye level a horizontal line. This is termed the *reduced vibrational density of states*. The BP has been observed in a number of glassy systems and is often quoted to be related to transversal modes [166–168], but the peak is also found in crystals where its intensity was found to scale with density [169]. For the studied CAS system such computation is presented in Figure 4.16a with a clear indication of a peak in the range of 1-4 THz (higher peak frequency with higher pressure).

In addition to the simulated BPs, we performed THz time-domain spectroscopy measurements of the pristine and 1 GPa hot compressed experimental CAS glasses to qualitatively confirm the trend of the simulations. As shown in the inset of Figure 4.16a, the trend of the simulations with decreasing intensity and increasing peak frequency was confirmed by the experiments. Now, while the CAS system under pressure features a clear boson peak behavior, it may be surprising that by normalization with the Debye frequency [169], it is possible to collapse both the frequency and intensity onto a single curve for nearly all studied glasses as shown in Figure 4.16b. This points towards that the changes of the BS is governed by simple transformations of the elastic medium as described by Debye theory. In extension to the found correlation with the Debye theory, it is furthermore found that the BP frequency correlates very nicely with the total thermal conductivity (see Figure 4.16c). A similar correlation is found to exist for the simple binary series of lithium borates as obtained from the literature (Figure 4.16c) [12, 170]. As the BP both correlates with the Debye frequency and κ, the results now imply, that Debye frequency and κ also correlate. This is an interesting finding for the fundamental understanding of κ. Now, it may be worth embracing how the Debye frequency (ω_{D}) is origi-

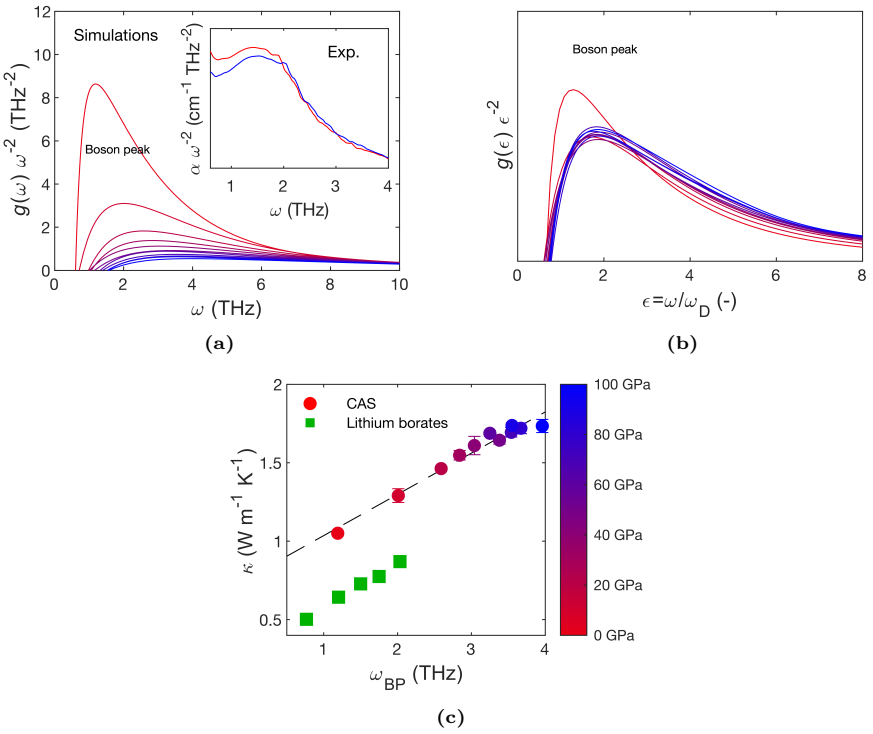

Fig. 4.16: (a) Reduced vibrational density of states as well as (b) the reduced vibrational density of states rescaled with the Debye frequency. (c) Correlation between peak frequency of the boson peak (ω_{BP}) and total thermal conductivity in the studied compressed 30CaO-10Al_2O_3-60SiO_2 glasses from 0 to 100 GPa. The inset of (a) shows the reduced absorption coefficient of uncompressed and hot compressed (to 1 GPa) 30CaO-10Al_2O_3-60SiO_2 glass as obtained from THz time-domain spectroscopy. Figures (a), (b), and (c) are reprinted from Paper V.

nally defined, namely, as a cutoff frequency of the VDOS in the Debye model. Increasing ω_D will thus correspond to increasing the cutoff in the VDOS and hence enlarge the frequency span of modes participating in the vibrations of the structure. Phenomenologically this is much like the observed transformation of higher frequency modes which start as localized and turn into extended modes when increasing the pressure as shown in Figure 4.14. This transformation is then causing a significant increase in the diffusivity of higher-frequency modes, effectively governing the shown increase in κ. In addition to the correlations build in Section 4.1, these newly developed correlations with the BP and ω_D may aid in the making of more comprehensive models for describing heat transfer in oxide glasses and glasses in general.

Chapter 5

Conclusions

The presented thesis has explored structural and thermal characterization of oxide based glasses. A comprehensive introduction to oxide glass structure has been given (Paper I), including an introduction to the recent method of persistent homology (Paper II). Additionally, the fundamental heat transfer properties of glasses, and in particularly oxide glasses, have been studied. However, the main outcome of the present thesis is that of the coupling between thermal conductivity and structure in oxide glasses.

Specifically, while there exist a number of studies of thermal conductivity in oxide glass systems, they are often dedicated to either low temperature anomalies or providing simple empirical multiple-regression correlations for use in glass engineering. While the former is mainly of interest for fundamental physics, the latter attempts of predicting thermal conductivity have been fundamentally flawed. As such, this thesis has been devoted to establishing structural correlations to thermal conductivity.

To establish such correlations, a number of glass systems with anomalous coordination number changes have been studied, including two series of soda lime borosilicate (Paper III) and lithium germanate (Paper IV) glasses, respectively. Here, boron was able to change coordination number from 3 to 4, while germanium could see coordination numbers in the range of 4 and 5 and/or 6. It was found that thermal conductivity in some cases see correlation with simple coordination number metrics, however that this was not always the case.

Now, instead of focusing on a direct correlation between the total thermal conductivity and a simple structural metric like the coordination number, more detailed approaches were taken. It was shown how the contribution of thermal conductivity could be split into two contributions, namely those of propagative and diffusive modes. The latter was obtained from a simple semi-empirical correlation with inputs of temperature, atomic number density, and average speed

of sound. Generally, increasing either atomic number density or sound speed provides increasing diffuson contribution to thermal conductivity. With measurements of the total thermal conductivity it was then possible to establish a measure of the contribution of propagative modes to thermal conductivity as a simple difference between the total and diffusive contribution to thermal conductivity. By performing such analysis for a number of oxide glasses in the silicate, borate, germanate, and borosilicate families, it was possible to establish a correlation between the propagon contribution to thermal conductivity and the number of atomic constraints per unit volume as obtained from topological constraint theory. While the correlation varied with glass family, it was positive for all studied glass series. Further work is required to actively explain the differences in the correlation between volumetric constraint density and the contribution of propagons to total thermal conductivity. These results allow for summarizing a few guidelines for increasing thermal conductivity of oxide glass systems, namely: i) Choose low molecular weight constituents for increasing atomic number density; ii) choose high field strength ions to increase sound speed; and iii) maximize glass rigidity

In addition to the experimentally based studies on oxide glasses and the establishment of semi-empirical correlations between thermal conductivity and glass structure, a detailed study of a series of compressed (from 0 to 100 GPa) calcium aluminosilicate glasses was performed and included in the present thesis as Paper V. Through the use of a recently developed method for estimating thermal conductivity based on lattice dynamics, it was shown how the glasses saw great increases of thermal conductivity with increasing pressure, originating from changes in the mode diffusivity of high frequency (>15 THz) modes. This change was accompanied by a significant increase in the participation ratio of these modes, ultimately following a relation governed by simple coordination number changes of especially the main constituents of the glass, i.e., oxygen and silicon. Lastly, it was shown how thermal conductivity and the boson peak frequency was closely coupled and scaled very well with the Debye frequency. This ultimately suggests that the thermal conductivity in the studied oxide system scale with the simple transformation of the elastic medium, as governed by Debye theory.

Chapter 6

Perspectives

While this thesis has explored structure-heat transfer correlations in oxide glasses and established some preliminary correlations between these parameters, more work is required to fully enlighten the sought correlations. For example, a number of questions have arisen upon the presented results;

- How can the differences in the propagon contribution to thermal conductivity between glass families be explained?
- Is it possible to provide a physical argument to explain the differences in the propagon contribution to thermal conductivity between glass families?
- How are the found correlations affected by temperature?
- Do the found results extend to the case of the molten state?
- Which medium-range order structural features govern changes of thermal conductivity in the oxide glass family?
- How will pressure affect thermal conductivity in simple binary oxide glasses?
- Is it possible to correlate the boson peak frequency to thermal conductivity in general?

To answer these questions, further experimental and simulation-based studies of more oxide glasses are required. For experiments, this could include the tedious preparation of multiple series of oxide glasses of varying modifier ions to deduce the effect of network modifier on the correlation between constraint density and propagon contribution to thermal conductivity. Similar glass series could be exploited to further study the effect of pressure history on thermal conductivity. For the simulations, further studies of oxide systems using the

recent unified model of heat transfer would be of significant importance to confirm or deny if the found correlations depicted in Paper V are system-specific or generic, e.g., the found correlation between the boson peak, Debye frequency, and thermal conductivity. For more, it is believed that simulations will be the key for studying the effect of medium-range order structure and its correlation to thermal conductivity, e.g., by coupling persistent homology with different machine learning algorithms.

In conclusion, despite their vitreous state, this thesis has shown how the structure of oxide glass systems seems to greatly impact their heat transfer properties with clear connections to rigidity. This should allow for, at least qualitatively, tuning and optimizing the thermal conductivity in oxide glasses, and may pave the way for future studies to build quantitative models of heat transfer phenomena in these systems. This will ultimately aid in the development of future glass products as well as the fundamental understanding of the physics governing heat transfer in amorphous materials.

References

[1] J. D. Musgraves, J. Hu, and L. Calvez, *Springer Handbook of Glass*. Springer, 2019.

[2] A. K. Varshneya, *Fundamentals of inorganic glasses*. Society of Glass Technology, 2013.

[3] J. E. Shelby, *Introduction to Glass Science and Technology*. The Royal Society of Chemistry, 2nd ed., 2005.

[4] J. C. Mauro, C. S. Philip, D. J. Vaughn, and M. S. Pambianchi, "Glass science in the United States: Current status and future directions," *International Journal of Applied Glass Science*, vol. 5, no. 1, pp. 2–15, 2014.

[5] J. Ballato and P. Dragic, "Rethinking optical fiber: New demands, old glasses," *Journal of the American Ceramic Society*, vol. 96, no. 9, pp. 2675–2692, 2013.

[6] A. Ellison and I. A. Cornejo, "Glass Substrates for Liquid Crystal Displays," *International Journal of Applied Glass Science*, vol. 1, no. 1, pp. 87–103, 2010.

[7] M. C. Wingert, J. Zheng, S. Kwon, and R. Chen, "Thermal transport in amorphous materials: A review," *Semiconductor Science and Technology*, vol. 31, p. 113003, 2016.

[8] D. L. Morse and J. W. Evenson, "Welcome to the Glass Age," *International Journal of Applied Glass Science*, vol. 7, no. 4, pp. 409–412, 2016.

[9] J. C. Mauro, A. Tandia, K. D. Vargheese, Y. Z. Mauro, and M. M. Smedskjaer, "Accelerating the Design of Functional Glasses through Modeling," *Chemistry of Materials*, vol. 28, pp. 4267–4277, 2016.

[10] J. C. Mauro, "Topological constraint theory of glass," *American Ceramic Society Bulletin*, vol. 90, no. 4, pp. 31–37, 2011.

[11] S. He, Y. Li, L. Liu, Y. Jiang, J. Feng, W. Zhu, J. Zhang, Z. Dong, Y. Deng, J. Luo, W. Zhang, and G. Chen, "Semiconductor glass with superior flexibility and high room temperature thermoelectric performance," *Science Advances*, vol. 6, p. eaaz8423, 2020.

[12] S. S. Sørensen, H. Johra, J. C. Mauro, M. Bauchy, and M. M. Smedskjaer, "Boron anomaly in the thermal conductivity of lithium borate glasses," *Physical Review Materials*, vol. 3, no. 7, p. 075601, 2019.

[13] S. S. Sørensen, E. J. Pedersen, F. K. Paulsen, I. H. Adamsen, J. L. Laursen, S. Christensen, H. Johra, L. R. Jensen, and M. M. Smedskjaer, "Heat conduction in oxide glasses: Balancing diffusons and propagons by network rigidity," *Applied Physics Letters*, vol. 117, p. 031901, 2020.

[14] S. S. Sørensen, C. A. N. Biscio, M. Bauchy, L. Fajstrup, and M. M. Smedskjaer, "Revealing hidden medium-range order in amorphous materials using topological data analysis," *Science Advances*, vol. 6, p. eabc2320, 2020.

[15] S. S. Sørensen, M. B. Østergaard, M. Stepniewska, H. Johra, Y. Yue, and M. M. Smedskjaer, "Metal-Organic Framework Glasses possess Higher Thermal Conductivity than their Crystalline Counterparts," *ACS Applied Materials and Interfaces*, vol. 12, pp. 18893–18903, 2020.

[16] C. Kittel, *Introduction to Solid State Physics*. Wiley, 8th ed., 2005.

[17] P. Atkins and J. d. Paula, *Atkins' Physical Chemistry*. Oxford University Press, 10th ed., 2014.

[18] W. H. Zachariasen, "The atomic arrangement in glass," *Journal of the American Chemical Society*, vol. 54, no. 10, pp. 3841–3851, 1932.

[19] S. R. Elliott, "Origin of the First Sharp Diffraction Peak in the Structure Factor of Covalent Glasses," *Physical Review Letters*, vol. 67, no. 6, pp. 711–714, 1991.

[20] A. Dietzel, "Die kationenfeldstärken und ihre beziehungen zu entglasungsvorgängen, zur verbindungsbildung und schmelzpunkten von silikaten," *Z. Elektrochem. Angew. Phys. Chem.*, vol. 48, no. 1, pp. 9–23, 1942.

[21] B. E. Warren and J. Biscoe, "Fourier Analysis of X-ray patterns of soda-silica glass," *Journal of the American Ceramic Society*, vol. 21, no. 7, pp. 259–265, 1938.

[22] G. Greaves, "EXAFS and the structure of glass," *Journal of Non-Crystalline Solids*, vol. 71, pp. 203–217, 1985.

[23] G. N. Greaves, A. Fontaine, P. Lagarde, D. Raoux, and S. J. Gurman, "Local structure of silicate glasses," *Nature*, vol. 293, pp. 611–616, 1981.

[24] R. Dupree, D. Holland, and M. G. Mortuza, "Six-coordinated silicon in glasses," *Nature*, vol. 328, pp. 416–417, 1987.

[25] C. Prescher, V. B. Prakapenka, J. Stefanski, S. Jahn, L. B. Skinner, and Y. Wang, "Beyond sixfold coordinated Si in SiO_2 glass at ultrahigh pressures," *Proceedings of the National Academy of Sciences of the United States of America*, vol. 114, no. 38, pp. 10041–10046, 2017.

[26] P. J. Bray and J. G. O'Keeffe, "Nuclear magnetic resonance investigations of the structure of alkali borate glasses," *Phys. Chem. Glasses*, vol. 4, pp. 37–46, 1963.

[27] A. C. Hannon, D. Di Martino, L. F. Santos, and R. M. Almeida, "A model for the Ge-O coordination in germanate glasses," *Journal of Non-Crystalline Solids*, vol. 353, no. 18-21, pp. 1688–1694, 2007.

[28] R. S. Welch, C. J. Wilkinson, Y. T. Shih, M. S. Bødker, A. V. DeCeanne, M. M. Smedskjaer, L. Huang, M. Affatigato, S. A. Feller, and J. C. Mauro, "Topological model of alkali germanate glasses and exploration of the germanate anomaly," *Journal of the American Ceramic Society*, vol. 103, pp. 4224–4233, 2020.

[29] G. S. Henderson and H. M. Wang, "Germanium coordination and the germanate anomaly," *European Journal of Mineralogy*, vol. 14, no. 4, pp. 733–744, 2002.

[30] S. K. Lee, K. Y. Mun, Y. H. Kim, J. Lhee, T. Okuchi, and J. F. Lin, "Degree of Permanent Densification in Oxide Glasses upon Extreme Compression up to 24 GPa at Room Temperature," *Journal of Physical Chemistry Letters*, vol. 11, no. 8, pp. 2917–2924, 2020.

[31] S. Kapoor, L. Wondraczek, and M. M. Smedskjaer, "Pressure-induced densification of oxide glasses at the glass transition," *Frontiers in Materials*, vol. 4, p. 1, 2017.

[32] V. V. Brazhkin, I. Farnan, K. I. Funakoshi, M. Kanzaki, Y. Katayama, A. G. Lyapin, and H. Saitoh, "Structural transformations and anomalous viscosity in the B_2O_3 melt under high pressure," *Physical Review Letters*, vol. 105, p. 115701, 2010.

[33] T. Deschamps, J. Margueritat, C. Martinet, A. Mermet, and B. Champagnon, "Elastic moduli of permanently densified silica glasses," *Scientific Reports*, vol. 4, p. 7193, 2014.

[34] M. Murakami, S. Kohara, N. Kitamura, J. Akola, H. Inoue, A. Hirata, Y. Hiraoka, Y. Onodera, I. Obayashi, J. Kalikka, N. Hirao, T. Musso, A. S. Foster, Y. Idemoto, O. Sakata, and Y. Ohishi, "Ultrahigh-pressure form of SiO_2 glass with dense pyrite-type crystalline homology," *Physical Review B*, vol. 99, p. 045153, 2019.

[35] Y. Kono, Y. Shu, C. Kenney-Benson, Y. Wang, and G. Shen, "Structural Evolution of SiO_2 Glass with Si Coordination Number Greater than 6," *Physical Review Letters*, vol. 125, no. 20, p. 205701, 2020.

[36] G. Spiekermann, M. Harder, K. Gilmore, P. Zalden, C. J. Sahle, S. Petitgirard, M. Wilke, N. Biedermann, C. Weis, W. Morgenroth, J. S. Tse, E. Kulik, N. Nishiyama, H. Yavaş, and C. Sternemann, "Persistent Octahedral Coordination in Amorphous GeO2 Up to 100 GPa by Kβ" X-Ray Emission Spectroscopy," *Physical Review X*, vol. 9, p. 011025, 2019.

[37] Y. Kono, C. Kenney-Benson, D. Ikuta, Y. Shibazaki, Y. Wang, G. Shen, and A. Navrotsky, "Ultrahigh-pressure polyamorphism in GeO_2 glass with coordination number >6," *Proceedings of the National Academy of Sciences of the United States of America*, vol. 113, no. 13, pp. 3436–3441, 2016.

[38] S. K. Lee, P. J. Eng, H. K. Mao, Y. Meng, M. Newville, M. Y. Hu, and J. Shu, "Probing of bonding changes in B_2O_3 glasses at high pressure with inelastic X-ray scattering," *Nature Materials*, vol. 4, no. 11, pp. 851–854, 2005.

[39] S. K. Lee, Y. H. Kim, P. Chow, Y. Xiao, C. Ji, and G. Shen, "Amorphous boron oxide at megabar pressures via inelastic X-ray scattering," *Proceedings of the National Academy of Sciences of the United States of America*, vol. 115, no. 23, pp. 5855–5860, 2018.

[40] J. F. Stebbins and S. Bista, "Pentacoordinated and hexacoordinated silicon cations in a potassium silicate glass: Effects of pressure and temperature," *Journal of Non-Crystalline Solids*, vol. 505, pp. 234–240, 2019.

[41] S. K. Lee, A. C. Lee, and J. J. Kweon, "Probing Medium-Range Order in Oxide Glasses at High Pressure," *Journal of Physical Chemistry Letters*, vol. 12, no. 4, pp. 1330–1338, 2021.

[42] M. Guerette, M. R. Ackerson, J. Thomas, F. Yuan, E. B. Watson, D. Walker, and L. Huang, "Structure and Properties of Silica Glass Densified in Cold Compression and Hot Compression," *Scientific Reports*, vol. 5, p. 15343, 2015.

[43] M. Guerette, M. R. Ackerson, J. Thomas, E. B. Watson, and L. Huang, "Thermally induced amorphous to amorphous transition in hot-compressed silica glass," *Journal of Chemical Physics*, vol. 148, no. 19, p. 194501, 2018.

[44] O. Benzine, Z. Pan, C. Calahoo, M. Bockowski, M. M. Smedskjaer, W. Schirmacher, and L. Wondraczek, "Vibrational disorder and densification-induced homogenization of local elasticity in silicate glasses," *Scientific Reports*, vol. 11, p. 24454, 2021.

[45] A. Zeidler, K. Wezka, R. F. Rowlands, D. A. Whittaker, P. S. Salmon, A. Polidori, J. W. Drewitt, S. Klotz, H. E. Fischer, M. C. Wilding, C. L. Bull, M. G. Tucker, and M. Wilson, "High-pressure transformation of SiO_2 glass from a tetrahedral to an octahedral network: A joint approach using neutron diffraction and molecular dynamics," *Physical Review Letters*, vol. 113, no. 3, p. 135501, 2014.

[46] Y. Yang, J. Zhou, F. Zhu, D. Chang, D. S. Kim, Y. Yuan, M. Pham, A. Rana, X. Tian, Y. Yao, S. Osher, L. Hu, P. Ercius, and J. Miao, "Determining the three-dimensional atomic structure of an amorphous solid," *Nature*, vol. 592, pp. 60–64, 2021.

[47] Q. Zhou, Y. Shi, B. Deng, J. Neuefeind, and M. Bauchy, "Experimental method to quantify the ring size distribution in silicate glasses and simulation validation thereof," *Science Advances*, vol. 7, p. eabh1761, 2021.

[48] P. Y. Huang, S. Kurasch, A. Srivastava, V. Skakalova, J. Kotakoski, A. V. Krasheninnikov, R. Hovden, Q. Mao, J. C. Meyer, J. Smet, D. A. Muller, and U. Kaiser, "Direct imaging of a two-dimensional silica glass on graphene," *Nano Letters*, vol. 12, no. 2, pp. 1081–1086, 2012.

[49] P. Debye, "Zerstreuung von Röntgenstrahlen," *Annalen der Physik*, vol. 351, no. 6, pp. 809–823, 1915.

[50] P. Scardi, S. J. Billinge, R. Neder, and A. Cervellino, "Celebrating 100 years of the Debye scattering equation," *Acta Crystallographica Section A: Foundations and Advances*, vol. 72, no. 6, pp. 589–590, 2016.

[51] F. Zernike and J. A. Prins, "Die Beugung von Röntgenstrahlen in Flüssigkeiten als Effekt der Molekülanordnung [The diffraction of x-rays in liquids as an effect of the molecular arrangement]," *Zeitschrift für Physik*, vol. 41, no. 2-3, pp. 184–194, 1927.

[52] S. R. Elliott, *Physics of Amorphous Materials*. Longman Publishing Group, 1st ed., 1983.

[53] D. A. Keen, "A comparison of various commonly used correlation functions for describing total scattering," *Journal of Applied Crystallography*, vol. 34, pp. 172–177, 2001.

[54] Q. Mei, C. J. Benmore, S. Sen, R. Sharma, and J. L. Yarger, "Intermediate range order in vitreous silica from a partial structure factor analysis," *Physical Review B*, vol. 78, p. 144204, 2008.

[55] M. Edén, "NMR studies of oxide-based glasses," *Annual Reports on the Progress of Chemistry - Section C*, vol. 108, pp. 177–221, 2012.

[56] R. Youngman, "NMR spectroscopy in glass science: A review of the elements," *Materials*, vol. 11, p. 476, 2018.

[57] H. Friebolin and J. K. Becconsall, *Basic one-and two-dimensional NMR spectroscopy*, vol. 7. Wiley-vch Weinheim:, 2005.

[58] L. Cormier, D. R. Neuville, and G. Calas, "Structure and properties of low-silica calcium aluminosilicate glasses," *Journal of Non-Crystalline Solids*, vol. 274, pp. 110–114, 2000.

[59] M. T. Dove, *Introduction to Lattice Dynamics*. Cambridge University Press, 1st ed., 1993.

[60] C. F. Geraldes, "Introduction to infrared and raman-based biomedical molecular imaging and comparison with other modalities," *Molecules*, vol. 25, p. 5547, 2020.

[61] S. Speziale, H. Marquardt, and T. S. Duffy, "Brillouin scattering and its application in geosciences," *Reviews in Mineralogy and Geochemistry*, vol. 78, pp. 543–603, 2014.

[62] J. C. Phillips, "Topology of covalent non-crystalline solids: Short-range order in chalcogenide alloys," *Journal of Non-Crystalline Solids*, vol. 34, pp. 153–181, 1979.

[63] M. F. Thorpe, "Continuous deformations in random networks," *Journal of Non-Crystalline Solids*, vol. 57, no. 3, pp. 355–370, 1983.

[64] M. Bauchy, "Deciphering the atomic genome of glasses by topological constraint theory and molecular dynamics: A review," *Computational Materials Science*, vol. 159, no. November 2018, pp. 95–102, 2019.

[65] Y. Wang, P. Boolchand, and M. Micoulaut, "Glass structure, rigidity transitions and the intermediate phase in the Ge-As-Se ternary," *Europhysics Letters*, vol. 52, no. 6, pp. 633–639, 2000.

[66] J. C. Mauro, P. K. Gupta, and R. J. Loucks, "Composition dependence of glass transition temperature and fragility. II. A topological model of alkali borate liquids," *Journal of Chemical Physics*, vol. 130, p. 234503, 2009.

[67] M. M. Smedskjaer, J. C. Mauro, and Y. Yue, "Prediction of glass hardness using temperature-dependent constraint theory," *Physical Review Letters*, vol. 105, p. 115503, 2010.

[68] M. M. Smedskjaer, J. C. Mauro, R. E. Youngman, C. L. Hogue, M. Potuzak, and Y. Yue, "Topological principles of borosilicate glass chemistry," *Journal of Physical Chemistry B*, vol. 115, no. 44, pp. 12930–12946, 2011.

[69] M. M. Smedskjaer, "Topological model for boroaluminosilicate glass hardness," *Frontiers in Materials*, vol. 1, p. 23, 2014.

[70] C. Hermansen, B. P. Rodrigues, L. Wondraczek, and Y. Yue, "An extended topological model for binary phosphate glasses," *Journal of Chemical Physics*, vol. 141, p. 244502, 2014.

[71] C. Hermansen, R. E. Youngman, J. Wang, and Y. Yue, "Structural and topological aspects of borophosphate glasses and their relation to physical properties," *Journal of Chemical Physics*, vol. 142, p. 184503, 2015.

[72] C. Hermansen, X. Guo, R. E. Youngman, J. C. Mauro, M. M. Smedskjaer, and Y. Yue, "Structure-topology-property correlations of sodium phosphosilicate glasses," *Journal of Chemical Physics*, vol. 143, p. 064510, 2015.

[73] L. Verlet, "Computer "Experiments" on Classical Fluid. I. Thermodynamical Properties of Lennard-Jones Molecules," *Physical Review*, vol. 159, no. 1, pp. 98–103, 1967.

[74] J. Du, "Challenges in Molecular Dynamics Simulations of Multicomponent Oxide Glasses," in *Molecular Dynamics Simulations of Disordered Materials*, pp. 157–180, Springer, 2015.

[75] A. Pedone, M. Bertani, L. Brugnoli, and A. Pallini, "Interatomic potentials for oxide glasses: Past, present, and future," *Journal of Non-Crystalline Solids: X*, vol. 15, no. June, p. 100115, 2022.

[76] L. Pedesseau, S. Ispas, and W. Kob, "First-principles study of a sodium borosilicate glass-former. II. the glass state," *Physical Review B*, vol. 91, no. 13, p. 134202, 2015.

[77] S. Sundararaman, L. Huang, S. Ispas, and W. Kob, "New interaction potentials for borate glasses with mixed network formers," *Journal of Chemical Physics*, vol. 152, p. 104501, 2019.

[78] Y. Onodera, S. Kohara, P. S. Salmon, A. Hirata, N. Nishiyama, S. Kitani, A. Zeidler, M. Shiga, A. Masuno, H. Inoue, S. Tahara, A. Polidori, H. E. Fischer, T. Mori, S. Kojima, H. Kawaji, A. I. Kolesnikov, M. B. Stone, M. G. Tucker, M. T. McDonnell, A. C. Hannon, Y. Hiraoka, I. Obayashi, T. Nakamura, J. Akola, Y. Fujii, K. Ohara, T. Taniguchi, and O. Sakata, "Structure and properties of densified silica glass: characterizing the order within disorder," *NPG Asia Materials*, vol. 12, p. 85, 12 2020.

[79] Y. Hiraoka, T. Nakamura, A. Hirata, E. G. Escolar, K. Matsue, and Y. Nishiura, "Hierarchical structures of amorphous solids characterized by persistent homology," *Proceedings of the National Academy of Sciences*, vol. 113, no. 26, pp. 7035–7040, 2016.

[80] H. Edelsbrunner and J. Harer, *Computational topology: an introduction*. American Mathematical Society, 2009.

[81] Y. Lee, S. D. Barthel, P. Dłotko, S. M. Moosavi, K. Hess, and B. Smit, "Quantifying similarity of pore-geometry in nanoporous materials," *Nature Communications*, vol. 8, p. 15396, 2017.

[82] A. S. Krishnapriyan, M. Haranczyk, and D. Morozov, "Topological Descriptors Help Predict Guest Adsorption in Nanoporous Materials," *Journal of Physical Chemistry C*, vol. 124, no. 17, pp. 9360–9368, 2020.

[83] E. Minamitani, T. Shiga, M. Kashiwagi, and I. Obayashi, "Topological descriptor of thermal conductivity in amorphous materials," *The Journal of Chemical Physics*, vol. 156, p. 244502, 2022.

[84] G. S. Nolas and H. J. Goldsmid, "The figure of merit in amorphous thermoelectrics," *Physica Status Solidi (A) Applied Research*, vol. 194, no. 1, pp. 271–276, 2002.

[85] M. K. Choudhary and R. M. Potter, "Heat transfer in glass-forming melts," in *Properties of Glass-Forming Melts* (L. D. Pye, A. Montenero, and I. Joseph, eds.), ch. 9, CRC Press, Taylor and Francis, 2005.

[86] A. Eucken, "Über die Temperaturabhängigkeit der Wärmeleitfähigkeit fester Nichtmetalle," *Annalen der Physik*, vol. 34, no. 2, p. 185, 1911.

[87] R. Peierls, "Zur kinetischen Theorie der Wärmeleitung in Kristallen," *Annalen der Physik*, vol. 395, no. 8, pp. 1055–1101, 1929.

[88] P. G. Klemens, "The thermal conductivities of some dielectric solids at low temperatures," *Proceedings of the Royal Society of London. Series A. Mathematical and Physical Sciences.*, vol. 208, no. 1092, pp. 108–133, 1951.

[89] C. Kittel, "Interpretation of the Thermal Conductivity of Glasses," *Physical Review*, vol. 75, no. 6, pp. 972–974, 1949.

[90] O. Andersson and H. Suga, "Thermal conductivity of amorphous ices," *Physical Review B*, vol. 65, no. 14, p. 140201, 2002.

[91] D. . R. Lide, *CRC handbook of chemistry and physics*. CRC Press, 86th ed., 2005.

[92] H. Wada and T. Kamijoh, "Thermal Conductivity of Amorphous Silicon," *Japanese Journal of Applied Physics*, vol. 35, no. 2, pp. 648–650, 1996.

[93] S. Cheng, X. Shi, W. Ma, X. Zhang, G. Liu, M. Pan, and W. Wang, "Experimental research on thermal transport properties of crystallized palladium-based alloys," *Frontiers in Energy*, vol. 12, no. 1, pp. 121–126, 2018.

[94] K. Eiermann, "Thermal Conductivity of High Polymers," *Journal of Polymer Science Part C*, vol. 6, no. 1, pp. 157–165, 1964.

[95] N. C. Shukla, H. H. Liao, J. T. Abiade, F. Liu, P. K. Liaw, and S. T. Huxtable, "Thermal conductivity and interface thermal conductance of amorphous and crystalline $Zr_{47}Cu_{31}Al_{13}Ni_9$ alloys with a Y_2O_3 coating," *Applied Physics Letters*, vol. 94, no. 8, p. 081912, 2009.

[96] C. L. Choy and K. Young, "Thermal conductivity of semicrystalline polymers - a model," *Polymer*, vol. 18, no. 8, pp. 769–776, 1977.

[97] R. C. Zeller and R. O. Pohl, "Thermal conductivity and specific heat of non-crystalline solids," *Phys. Rev. B*, vol. 4, no. 6, pp. 2029–2041, 1971.

[98] M. Beekman and D. G. Cahill, "Inorganic Crystals with Glass-Like and Ultralow Thermal Conductivities," *Crystal Research and Technology*, vol. 52, no. 10, p. 1700114, 2017.

[99] P. W. Anderson, "Absence of diffusion in certain random lattices," *Physical Review*, vol. 109, no. 5, pp. 1492–1505, 1958.

[100] A. Einstein, "Elementare Betrachtungen über die thermlsche Molecularbewegung in festen Körpern," *Annalen der Physik*, vol. 35, p. 679, 1911.

[101] D. G. Cahill, S. K. Watson, and R. O. Pohl, "Lower limit to the thermal conductivity of disordered crystals," *Physical Review B*, vol. 46, no. 10, pp. 6131–6140, 1992.

[102] P. B. Allen and J. L. Feldman, "Thermal Conductivity of Glasses: Theory and Application to Amorphous Si," *Physical Review Letters*, vol. 62, no. 6, pp. 645–648, 1989.

[103] P. B. Allen and J. L. Feldman, "Thermal conductivity of disordered harmonic solids," *Physical Review B*, vol. 48, no. 17, pp. 12581–12588, 1993.

[104] P. B. Allen, J. L. Feldman, J. Fabian, and F. Wooten, "Diffusons, locons and propagons: Character of atomic vibrations in amorphous Si," *Philosophical Magazine B*, vol. 79, pp. 1715–1731, 1999.

[105] H. R. Seyf and A. Henry, "A method for distinguishing between propagons, diffusions, and locons," *Journal of Applied Physics*, vol. 120, p. 025101, 2016.

[106] S. Kommandur and S. K. Yee, "An empirical model to predict temperature-dependent thermal conductivity of amorphous polymers," *Journal of Polymer Science, Part B: Polymer Physics*, vol. 55, no. 15, pp. 1160–1170, 2017.

[107] M. T. Agne, R. Hanus, and G. J. Snyder, "Minimum thermal conductivity in the context of diffuson-mediated thermal transport," *Energy and Environmental Science*, vol. 11, no. 3, pp. 609–616, 2018.

[108] M. Simoncelli, N. Marzari, and F. Mauri, "Unified theory of thermal transport in crystals and disordered solids," *Nature Physics*, vol. 15, pp. 809–813, 2019.

[109] L. Isaeva, G. Barbalinardo, D. Donadio, and S. Baroni, "Modeling heat transport in crystals and glasses from a unified lattice-dynamical approach," *Nature Communications*, vol. 10, p. 3853, 2019.

[110] M. Matsui, "Molecular dynamics study of the structures and bulk moduli of crystals in the system CaO-MgO-Al_2O_3-SiO_2," *Physics and Chemistry of Minerals*, vol. 23, no. 6, pp. 345–353, 1996.

[111] J. Zhao, P. H. Gaskell, L. Cormier, and S. M. Bennington, "Vibrational density of states and structural origin of the heat capacity anomalies in $Ca_3Al_2Si_3O_{12}$ glasses," *Physica B*, vol. 241-243, pp. 906–908, 1998.

[112] Y. Tian, J. Du, W. Han, X. Zu, X. Yuan, and W. Zheng, "Thermal conductivity of vitreous silica from molecular dynamics simulations: The effects of force field, heat flux and system size," *Journal of Chemical Physics*, vol. 146, p. 054504, 2017.

[113] E. S. Toberer, L. L. Baranowski, and C. Dames, "Advances in Thermal Conductivity," *Annual Review of Materials Research*, vol. 42, no. 1, pp. 179–209, 2012.

[114] W. J. Parker, R. J. Jenkins, C. P. Butler, and G. L. Abbott, "Flash Method of Determining Thermal Diffusivity, Heat Capacity, and Thermal Conductivity," *Journal of Applied Physics*, vol. 32, no. 9, pp. 1679–1684, 1961.

[115] R. D. Cowan, "Pulse method of measuring thermal diffusivity at high temperatures," *Journal of Applied Physics*, vol. 34, no. 4, pp. 926–927, 1963.

[116] D. G. Cahill and R. O. Pohl, "Thermal conductivity of amorphous solids above the plateau," *Physical Review B*, vol. 35, no. 8, pp. 4067–4073, 1987.

[117] W. Zhou, Y. Cheng, K. Chen, G. Xie, T. Wang, and G. Zhang, "Thermal Conductivity of Amorphous Materials," *Advanced Functional Materials*, vol. 30, no. 8, p. 1903829, 2019.

[118] F. Müller-Plathe, "A simple nonequilibrium molecular dynamics method for calculating the thermal conductivity," *The Journal of Chemical Physics*, vol. 106, no. 14, pp. 6082–6085, 1997.

[119] S. Ju, X. Liang, and X. Xu, "Out-of-plane thermal conductivity of polycrystalline silicon nanofilm by molecular dynamics simulation," *Journal of Applied Physics*, vol. 110, p. 054318, 2011.

[120] D. P. Sellan, E. S. Landry, J. E. Turney, A. J. H. McGaughey, and C. H. Amon, "Size effects in molecular dynamics thermal conductivity predictions," *Physical Review B*, vol. 81, no. 21, p. 214305, 2010.

[121] M. S. Green, "Markoff random processes and the statistical mechanics of time-dependent phenomena. II. Irreversible processes in fluids," *The Journal of Chemical Physics*, vol. 22, no. 3, pp. 398–413, 1954.

[122] R. Kubo, M. Yokota, and S. Nakajima, "Statistical-Mechanical Theory of Irreversible Processes. II. Response to Thermal Disturbance," *Journal of the Physical Society of Japan*, vol. 12, no. 11, pp. 1203–1211, 1957.

[123] R. Kubo, "Statistical-Mechanical Theory of Irreversible Processes. I. General Theory and Simple Applications to Magnetic and Conduction Problems," *Journal of the Physical Society of Japan*, vol. 12, no. 6, pp. 570–586, 1957.

[124] R. J. Hardy, "Energy-Flux Operator for a Lattice," *Physical Review*, vol. 132, no. 1, p. 168, 1963.

[125] M. Bauchy, "Structural , vibrational , and elastic properties of a calcium aluminosilicate glass from molecular dynamics simulations : The role of the potential Structural , vibrational , and elastic properties of a calcium aluminosilicate glass from molecular dynamics," *Journal of Chemical Physics*, vol. 141, p. 024507, 2014.

[126] R. Christensen, S. S. Sørensen, H. Liu, K. Li, M. Bauchy, and M. M. Smedskjaer, "Interatomic potential parameterization using particle swarm optimization: Case study of glassy silica," *Journal of Chemical Physics*, vol. 154, p. 134505, 2021.

[127] A. Rohskopf, H. R. Seyf, K. Gordiz, T. Tadano, and A. Henry, "Empirical interatomic potentials optimized for phonon properties," *npj Computational Materials*, vol. 3, p. 27, 2017.

[128] P. F. van Velden, "Thermal conductivities of some lead and bismuth glasses," *Glass Technology*, vol. 6, pp. 166–169, 1965.

[129] M. Susa, M. Watanabe, S. Ozawa, and R. Endo, "Thermal conductivity of CaO–SiO_2–Al_2O_3 glassy slags: Its dependence on molar ratios of Al_2O_3/CaO and SiO_2/Al_2O_3," *Ironmaking & Steelmaking*, vol. 34, no. 2, pp. 124–130, 2007.

[130] M. M. Ammar, S. A. Gharib, M. M. Halawa, H. A. El-Batal, and K. El-Badry, "Thermal Conductivity of Silicate and Borate Glasses," *Communications of the American Ceramic Society*, vol. 66, no. 5, pp. 76–77, 1983.

[131] M. M. Ammar, M. M. Halawa, N. A. Ghoneim, A. F. Abbas, and H. A. El Batal, "Thermal Conductivity of Lead Borate Glasses," *Journal of the American Ceramic Society*, vol. 65, no. 10, pp. 174–175, 1982.

[132] M. M. Ammar, S. Gharib, K. El-Badry, N. A. Ghoneim, and H. A. El Batal, "Thermal Conductivity of Some Sodium Aluminosilicate Glasses," *Sprechsaal*, vol. 115, no. 8, pp. 692–693, 1982.

[133] S. Salman, N. Ghoneim, and S. Gharib, "Thermal conductivity of lithium iron silicate glasses," *Thermochimica Acta*, vol. 72, no. 3, pp. 269–276, 1984.

[134] S. N. Salama, S. M. Salman, and S. Gharib, "Thermal conductivity and their respective crystalline products," *Journal of Non-Crystalline Solids*, vol. 93, pp. 203–214, 1987.

[135] S. M. Salman and S. Gharib, "Some Physical Properties Concerning the Thermal Conductivity Data of BaO-Containing Silicate Glasses in Relation to Structure," *Thermochimica Acta*, vol. 82, pp. 345–355, 1984.

[136] Y. Hiroshima, Y. Hamamoto, S. Yoshida, and J. Matsuoka, "Thermal conductivity of mixed alkali silicate glasses at low temperature," *Journal of Non-Crystalline Solids*, vol. 354, pp. 341–344, 2008.

[137] N. A. Ghoneim and M. M. Halawa, "Effect of Boron Oxide on the Thermal Conductivity of some Sodium Silicate Glasses," *Thermochimica Acta*, vol. 83, pp. 341–345, 1985.

[138] N. A. Ghoneim, A. A. Ahmed, and S. Gharib, "Effect of transition metal oxides on the thermal conductivity of glass," *Thermochimica Acta*, vol. 71, no. 1-2, pp. 43–51, 1983.

[139] V. I. Primenko, "Theoretical Method of Determining the Temperature Dependence of the Thermal Conductivity of Glasses," *Wärme - und Stoffübertragung*, vol. 3, no. 5, pp. 17–18, 1980.

[140] H. Kiyohashi, N. Hayakawa, S. Aratani, and H. Masuda, "Thermal conductivity of heat-absorbed soda-lime-silicate glasses at high temperatures," *High Temperatures - High Pressures*, vol. 34, pp. 1395–1404, 2002.

[141] R. Terai, M. Hori, and H. Yamanaka, "Thermal Conductivity of Mixed -Alkali Glasses," *American Ceramic Society Bulletin*, vol. 58, no. 11, p. 1125, 1979.

[142] E. H. Ratcliffe, "A survey of most probable values for the thermal conductivies of glasses between about -150 and 100°C, including new data on twnety-two glasses and a working formula for the calculation of conductivity from composition," *Glass Technology*, vol. 4, no. 4, pp. 113–128, 1963.

[143] W. Lv and A. Henry, "Examining the Validity of the Phonon Gas Model in Amorphous Materials," *Scientific Reports*, vol. 6, p. 37675, 2016.

[144] T. R. Anthony, W. F. Banholzer, and J. F. Fleischer, "Thermal diffusitivity of isotopically enriched ^{12}C diamond," *Physical Review B*, vol. 42, no. 2, pp. 1104–1111, 1990.

[145] L. Wei, P. K. Kuo, R. L. Thomas, T. R. Anthony, and W. F. Banholzer, "Thermal conductivity of isotopically modified single crystal diamond," *Physical Review Letters*, vol. 70, no. 24, pp. 3764–3767, 1993.

[146] W. J. Dell, P. J. Bray, and S. Z. Xiao, "^{11}B NMR studies and structural modeling of Na_2O-B_2O_3-SiO_2 glasses of high soda content," *Journal of Non-Crystalline Solids*, vol. 58, pp. 1–16, 1983.

[147] S. A. Feller, W. J. Dell, and P. J. Bray, "^{10}B NMR studies of lithium borate glasses," *Journal of Non-Crystalline Solids*, vol. 51, pp. 21–30, 1982.

[148] M. Tohmori, T. Sugawara, S. Yoshida, and J. Matsuoka, "Thermal conductivity of sodium borate glasses at low temperature," *Physics and Chemistry of Glasses: European Journal of Glass Science and Technology Part B*, vol. 50, no. 6, pp. 358–360, 2009.

[149] Y. Kim and K. Morita, "Thermal Conductivity of Molten Li_2O-B_2O_3 and K_2O-B_2O_3 Systems," *Journal of the American Ceramic Society*, vol. 98, no. 12, pp. 3996–4002, 2015.

[150] J. Lorösch, M. Couzi, J. Pelous, R. Vacher, and A. Levasseur, "Brillouin and Raman scattering study of borate glasses," *Journal of Non-Crystalline Solids*, vol. 69, pp. 1–25, 1984.

[151] S. Inaba, S. Oda, and K. Morinaga, "Equation for Estimating the Thermal Diffusivity, Specific Heat and Thermal Conductivity of Oxide Glasses," *J. Japan Inst. Metals*, vol. 65, no. 8, pp. 680–687, 2001.

[152] M. Khanisanij and H. A. A. Sidek, "Elastic behavior of borate glasses containing lead and bismuth oxides," *Advances in Materials Science and Engineering*, vol. 2014, p. 452830, 2014.

[153] S. K. Ahmmad, N. Jabeen, S. T. Uddin Ahmed, S. A. Ahmed, and S. Rahman, "Artificial intelligence density model for oxide glasses," *Ceramics International*, vol. 47, pp. 7946–7956, 2021.

[154] Y. J. Hu, G. Zhao, M. Zhang, B. Bin, T. Del Rose, Q. Zhao, Q. Zu, Y. Chen, X. Sun, M. de Jong, and L. Qi, "Predicting densities and elastic moduli of SiO2-based glasses by machine learning," *npj Computational Materials*, vol. 6, p. 25, 2020.

[155] H. Liu, Z. Fu, K. Yang, X. Xu, and M. Bauchy, "Machine learning for glass science and engineering: A review," *Journal of Non-Crystalline Solids: X*, vol. 4, no. August, p. 100036, 2019.

[156] J. I. Gersten and F. W. Smith, *The Physics and Chemistry of Materials*. Wiley, 2001.

[157] K. Aryana, D. A. Stewart, J. T. Gaskins, J. Nag, J. C. Read, D. H. Olson, M. K. Grobis, and P. E. Hopkins, "Tuning network topology and vibrational mode localization to achieve ultralow thermal conductivity in amorphous chalcogenides," *Nature Communications*, vol. 12, p. 2817, 2021.

[158] M. G. Ghossoub, J. H. Lee, O. T. Baris, D. G. Cahill, and S. Sinha, "Percolation of thermal conductivity in amorphous fluorocarbons," *Physical Review B*, vol. 82, p. 195441, 2010.

[159] J. L. Braun, S. W. King, A. Giri, J. T. Gaskins, M. Sato, T. Fujiseki, H. Fujiwara, and P. E. Hopkins, "Breaking network connectivity leads to ultralow thermal conductivities in fully dense amorphous solids," *Applied Physics Letters*, vol. 109, p. 191905, 2016.

[160] Q. Zheng, Y. Yue, and J. C. Mauro, "Density of topological constraints as a metric for predicting glass hardness," *Applied Physics Letters*, vol. 111, p. 011907, 2017.

[161] R. D. Shannon, "Revised Effective Ionic Radii and Systematic Studies of Interatomic Distances in Halides and Chalcogenides," *Acta Crystallographica*, vol. A32, p. 751, 1976.

[162] J. Du and L. R. Corrales, "First sharp diffraction peak in silicate glasses: Structure and scattering length dependence," *Physical Review B*, vol. 72, p. 092201, 2005.

[163] M. Solvang, Y. Z. Yue, S. L. Jensen, and D. B. Dingwell, "Rheological and thermodynamic behaviors of different calcium aluminosilicate melts with the same non-bridging oxygen content," *Journal of Non-Crystalline Solids*, vol. 336, no. 3, pp. 179–188, 2004.

[164] D. R. Neuville, L. Cormier, and D. Massiot, "Al coordination and speciation in calcium aluminosilicate glasses: Effects of composition determined by ^{27}Al MQ-MAS NMR and Raman spectroscopy," *Chemical Geology*, vol. 229, no. 1-3, pp. 173–185, 2006.

[165] J. W. Drewitt, S. Jahn, C. Sanloup, C. De Grouchy, G. Garbarino, and L. Hennet, "Development of chemical and topological structure in aluminosilicate liquids and glasses at high pressure," *Journal of Physics Condensed Matter*, vol. 27, p. 105103, 2015.

[166] Y. M. Beltukov, C. Fusco, D. A. Parshin, and A. Tanguy, "Boson peak and Ioffe-Regel criterion in amorphous siliconlike materials: The effect of bond directionality," *Physical Review E*, vol. 93, p. 023006, 2016.

[167] Y. C. Hu and H. Tanaka, "Origin of the boson peak in amorphous solids," *Nature Physics*, vol. 18, no. 6, pp. 669–677, 2022.

[168] A. I. Chumakov, I. Sergueev, U. Van Bürck, W. Schirmacher, T. Asthalter, R. Rüffer, O. Leupold, and W. Petry, "Collective nature of the boson peak and universal transboson dynamics of glasses," *Physical Review Letters*, vol. 92, no. 24, p. 245508, 2004.

[169] A. Monaco, A. I. Chumakov, Y. Z. Yue, G. Monaco, L. Comez, D. Fioretto, W. A. Crichton, and R. Rüffer, "Density of vibrational states of a hyperquenched glass," *Physical Review Letters*, vol. 96, p. 205502, 2006.

[170] S. Kojima, V. N. Novikov, and M. Kodama, "Fast relaxation, boson peak, and anharmonicity in Li_2O-B_2O_3 glasses," *Journal of Chemical Physics*, vol. 113, no. 15, pp. 6344–6350, 2000.

Publication list

Journal publications (newest first)

S. S. Sørensen, T. Du, C. A. N. Biscio, L. Fajstrup, M. M. Smedskjær, "Persistent Homology: A Tool to Understand Medium-Range Order Glass Structure", **Journal of Non-Crystalline Solids X**, In review.

S. S. Sørensen, P. P. Cielecki, H. Johra, M. Bockowski, E. Skovsen, Y. Yue, M. M. Smedskjær, "Thermal conduction in a densified oxide glass: Insights from lattice dynamics", **Materials Today Communications**, vol. 32, pp. 104160, 2022.

N. Ma, R. Ohtani, H. M. Le, S. S. Sørensen, R. Ishikawa, S. Kawata, S. Bureekaew, S. Kosasang, Y. Kawazoe, K. Ohara, M. M. Smedskjær, S. Horike, "Exploration of glassy state in Prussian blue analogues", **Nature Communications**, vol. 13, pp. 4023, 2022.

T. Du[1], S. S. Sørensen[1], T. To[1], M. M. Smedskjær, "Oxide glasses under pressure: Recent insights from experiments and simulations", **Journal of Applied Physics**, vol. 131, pp. 170901, 2022.

A. Qiao[1], S. S. Sørensen[1], M. Stepniewska, C. A. N. Biscio, L. Fajstrup, Z. Wang, X. Zhang, L. Calvez, I. Hung, Z. Gan, M. M. Smedskjær, Y. Yue, "Hypersensitivity of the Glass Transition to Pressure History in a Metal-Organic Framework Glass", **Chemistry of Materials**, vol. 34, pp. 5030-5038, 2022.

S. S. Sørensen, T. To, J. F. S. Christensen, H. Johra, M. M. Smedskjær, "Impact of network topology on the thermal and mechanical properties of lithium germanate glasses", **Journal of the American Ceramic Society**, vol. 105, pp. 977, 2022.

T. Du, H. Liu, L. Tang, S. S. Sørensen, M. Bauchy, M. M. Smedskjær, "Predicting Fracture Propensity in Amorphous Alumina from Its Static Structure

[1]Equal contribution

Using Machine Learning", **ACS Nano**, vol. 15, pp. 17705, 2021.

J. F. S. Christensen, S. S. Sørensen, T. To, M. Bauchy, M. M. Smedskjær, "Toughening of soda-lime-silica glass by nanoscale phase separation : Molecular dynamics study", **Physical Review Materials**, vol. 5, pp. 093602, 2021.

M. M. Smedskjær & S. S. Sørensen, "A Glass Act", **Nature Chemistry**, vol. 13, pp. 723-724, 2021.

S. S. Sørensen, M. S. Bødker, H. Johra, R. E. Youngman, S. Logunov, M. Bockowski, S. J. Rzoska, J. C. Mauro, M. M. Smedskjær, "Thermal conductivity of densified borosilicate glasses", **Journal of Non-Crystalline Solids**, vol. 557, pp. 120644, 2021.

T. To, S. S. Sørensen, J. F. S. Christensen, R. Christensen, L. R: Jensen, M. Bockowski, M. Bauchy, M. M. Smedskjær, "Bond switching in Densified Oxide Glass Enables Record-High Fracture Toughness", **ACS Applied Materials and Interfaces**, vol. 13, pp. 17753-17765, 2021.

T. To[1], S. S. Sørensen[1], Y. Yue, M. M. Smedskjær, "Bond switching is responsible for nanoductility in zeolitic imidazolate framework glasses", **Dalton Transactions**, vol. 50, pp. 6126-6132, 2021.

R. Christensen, S. S. Sørensen, H. Liu, K. Li, M. Bauchy, M. M. Smedskjær, "Interatomic potential parameterization using particle swarm optimization: Case study of glassy silica", **Journal of Chemical Physics**, vol. 154, pp. 134505, 2021.

S. S. Sørensen, C. A. N. Biscio, M. Bauchy, L. Fajstrup, and M. M. Smedskjær, "Revealing Hidden Medium-Range Order in Amorphous Materials using Topological Data Analysis," *Science Advances*, vol. 6, eabc2320, 2020.

S. S. Sørensen, E. J. Pedersen, F. K. Paulsen, I. H. Adamsen, J. L. Laursen, S. Christensen, H. Johra, L. R. Jensen, M. M. Smedskjær, "Heat conduction in oxide glasses: Balancing diffusons and propagons by network rigidity," *Applied Physics Letters*, vol. 117, pp. 031901, 2020.

T. To[1], S. S. Sørensen[1], M. Stepniewska, A. Qiao, L. R. Jensen, M. Bauchy, Y. Yue, M. M. Smedskjær, "Fracture toughness of a metal–organic framework glass", **Nature Communications**, vol. 11, pp. 2593, 2020.

S. S. Sørensen, M. B. Østergaard, M. Stepniewska, H. Johra, Y. Yue, M. M. Smedskjær, "Metal-Organic Framework Glasses possess Higher Thermal Conductivity than Their Crystalline Counterparts," **ACS Applied Materials and Interfaces**, vol. 12, no. 16, pp. 18893–18903, 2020.

S. S. Sørensen, H. Johra, J. C. Mauro, M. Bauchy, M. M. Smedskjær, "Boron anomaly in the thermal conductivity of lithium borate glasses," **Physical Review Materials**, vol. 3, pp. 075601, 2019.

M. S. Bødker, S. S. Sørensen, J. C. Mauro, M. M. Smedskjær, "Predicting Composition-Structure Relations in Alkali Borosilicate Glasses Using Statistical Mechanics", **Frontiers in Materials**, vol. 6, pp. 175, 2019.

Conference contributions (newest first)

R. Christensen, S. S. Sørensen, H. Liu, K. Li, M- Bauchy, M. M. Smedskjær, "Interatomic potential parameterization using particle swarm optimization: Case study of glassy silica", **26th International Congress on Glass**, Berlin Germany, 2022

T. Du, S. S. Sørensen, M. Bauchy, M. M. Smedskjær, "Disordering of Metal-Organic Framework Crystals and Glasses upon Irradiation", **26th International Congress on Glass**, Berlin Germany, 2022

T. Du, H. Liu, L. Tang, S. S. Sørensen, M. Bauchy, M. M. Smedskjær, "Predicting Bond Switching and Fracture in Simulated Al_2O_3 Glass Using Machine Learning", **26th International Congress on Glass**, Berlin Germany, 2022

S. S. Sørensen, P. P. Cielecki, H. Johra, M. Bockowski, E. Skovsen, M. M. Smedskjær, "Correlating thermal conductivity of oxide glasses with modal characteristics and network topology", **Glass and Optical Materials Division Conference**, Baltimore USA, 2022

S. S. Sørensen, X. Ren, T. Du, L. R. Jensen, M. M. Smedskjær, "Water as a flux in a hybrid coordination network glass", **Glass and Optical Materials Division Conference**, Baltimore USA, 2022

S. S. Sørensen, Y. Shi, M. Juelsholt, L. R. Jensen, M. Bockowski, K. M. Ø. Jensen, M. M. Smedskjær, "Anomalous elasticity in hot-compressed sodium germanate glasses is linked to medium-range order changes", **International Year of Glass Meeting**, Aalborg Denmark, 2022

Z. Chen, T. Du, S. S. Sørensen, R. Christensen, Q. Zhang, L. R. Jensen, M. Bauchy, M. M. Smedskjær, "Atomistic origin of variation in toughness and ionic conductivity in lithium borophosphate glassy electrolytes", **International Year of Glass Meeting**, Aalborg Denmark, 2022

Y. Xiao, T. Du, S. S. Sørensen, Z. Chen, Q. Zhang, M. M. Smedskjær, "De-

ciphering the medium-range order of zinc phosphate glasses using persistent homology", **International Year of Glass Meeting**, Aalborg Denmark, 2022

E. J. Pedersen, T. To, J. F. S. Christensen, R. Christensen, S. S. Sørensen, L. R. Jensen, M. Bockowski, O. Magdysyuk, M. Diaz-Lopez, Y. Yue, M. M. Smedskjær, "Structural Origin of Pressure-Induced Increase in Fracture Toughness of Alkali Aluminoborate Glasses", **International Year of Glass Meeting**, Aalborg Denmark, 2022

S. S. Sørensen, M. B. Østergaard, M. Stepniewska, H. Johra, Y. Yue, M. M. Smedslkaer, "Thermal Conductivity of Zeolitic Imidazolate Framework Glasses", **Pacrim 14 conference**, online poster, 2021

S. S. Sørensen, C. A. N. Biscio, M. Bauchy, L. Fajstrup, M. M. Smedskjaer, "Understanding Medium-Range Order Structure of Glasses using Persistent Homology", **Pacrim 14 conference**, online oral presentation, 2021

M. M. Smedskjaer, T. To, S. S. Sørensen, M. Stepniewska, A. Qiao, L. R. Jensen, M. Bauchy, Y. Yue, "Fracture Toughness of a Metal-Organic Framework Glass", **Pacrim 14 conference**, online oral presentation, 2021

M. M. Smedskjaer, T. To, S. S. Sørensen, J. F. S. Christensen, R. Christensen, L. R. Jensen, M. Bockowski, M. Bauchy, "Improving the Fracture Toughness of Oxide Glasses through Bond Switching", **Pacrim 14 conference**, online oral presentation, 2021

M. M. Smedskjær, T. To, S. S. Sørensen, T. Du, Y. Yue, M. Bauchy, "Fracture Toughness of Zeolitic Imidazolate Framework Glasses: Invited Talk", **Materials Science and Technology 2021**, online oral presentation, 2021

M. M. Smedskjaer, S. S. Sørensen, C. A. N. Biscio, M. Bauchy, L. Fajstrup, "Looking for order in disorder: topological data analysis of glass structure: Invited Talk", **Materials Science and Technology 2021**, online oral presentation, 2021

T. To, S. S. Sørensen, M. Stepniewska, A. Qiao, L. R. Jensen, M. Bauchy, Y. Yue, M. M. Smedskjaer, "Fracture Toughness of a Metal-Organic Framework Glass", **Engineering Mechanics Institute Conference 2021**, online oral presentation, 2021

S. S. Sørensen, C. A. N. Biscio, M. Bauchy, L. Fajstrup, M. M. Smedskjaer, "Topological data analysis as a tool to analyze the structure of amorphous materials", **Timeman Virtual Seminar**, Online, 2020 (Invited)

M. S. Bødker, S. S. Sørensen, J. C. Mauro, R. E. Youngman, M. M Smedskjaer,

"Designing the Network Former Speciation in Oxide Glasses using Statistical Mechanics", **4th International Workshop on Glass and Entropy**, Jena, Germany, 2019

M. S. Bødker, S. S. Sørensen, M. M Smedskjaer, "Statistical Mechanical Approach to Predict the Structure Evolution in Borosilicate Glasses", **25th ICG Conference**, Boston, USA, 2019

ISSN (online): 2446-1636
ISBN (online): 978-87-7573-838-0

AALBORG UNIVERSITY PRESS